GRAVITY SURVEY OF THE SHALLA CALDERA AND ITS ENVIRONS FOR THE EXPLORATION OF GEOTHERMAL ENERGY

BY

HARBIE HUSSEN

A THESIS

SUBMITTED TO THE SCHOOL OF GRADUATE STUDIES IN PARTIAL FULFILLMENT OF THE REQUIREMENTS FOR THE DEGREE MASTER OF SCIENCE IN GEOPHYSICS

February 2001

Addis Ababa

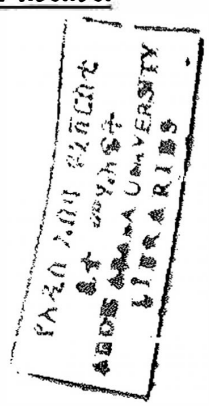

ACKNOWLEDGEMENTS

I am also grateful to Dr.Tigstu Haile, Dr.Gazehagn Yergu and Dr. Laike M. Asfaw for sharing their valuable time to go through the first draft and criticizing it constructively and guiding throughout the progress of the paper. I would like to thank Dr.Abera Alemu for his consent to use his compiled set of gravity data. I owe my thanks to Dr. Abebe Bekele, Dr. Tamiru Alemayohu, Dr. Endale Ketafo, Dr. Tesfaye Korme, Dr. Tenalem Ayenew and Dr. Ataley Ayele for their encouragement and advice.

I appreciate and thank the Ethiopian Geological Surveys and Aquatech private limited company for processing and reduction of the gravity data and for the use of Geosoft in the Geophysics department. I am indebted to all members of the Geophysics Department for their invaluable assistance. Special thanks are to Mogas Abera and Biniam Wondiradi for their friendly and invaluable assistance in using the software programs to prepare the different gravity anomaly maps.

The Oromia Water, Mineral and Energy Resources Development Bureau (OWMERDB) provided the Sponsorship and computer facility to print my thesis. My sincere thanks go to Juneyid Sado Ciri the former head of OWMERDB who encouraged and advised me to study geophysics. I am indebted to Tarku Negariti Negara, Kedir Abdela Geleta Gudeta, Mulalem Gazahegn, Likitu Dinagde and Ayanitu Bekele for their valuable assistance during the progress of my thesis.

ABSTRACT

For the possible assessment of geothermal resources it is necessary to obtain additional geophysical information from the gravity survey regarding the Shalla caldera and its environs. All available data, over 1041 stations, obtained from the EGS were reduced to sea level with a uniform crustal density of 2.67 gm/cm^3. Effects Bouguer masses were calculated applying the simple Bouguer correction. Terrain correction was not applied in which case its effect was treated as systematic error in computing the over all mean square error of the simple Bouguer anomalies at each station. Theoretical gravity field was computed by means of the international gravity formula of 1967 (GRS67) and tied to the IGSN71. The accuracy of the Bouguer anomaly at each station is calculated to about ± 2.82 mgal.

The data shows that the study area is characterised by short wavelength positive Bouguer gravity anomaly of the Ethiopian Rift. The observations define a line of positive residual gravity anomalies due to the mass excesses below the rift floor associated with strong hydrothermal activities in the rift. There is strong correlation between the positive residual gravity anomalies in the rift following the strike of the WFB, the geothermal activity and the location of Quaternary siliceous domes and recent fissural basalt flows. The root of the denser fissural basalt's may be still hot and the siliceous domes of the Shalla caldera geothermal field with strong hyrdrothermal manifestations more likely have hot basaltic dykes underneath associated with their magma chambers that feed their thermal features. In general all the geothermal activity north of Shalla caldera may be related with the Alutu-Langano geothermal field through the recent complex volcanic structures and the active trending fault system. Similarly the geothermal activity south of Shalla caldera may be ascribed to the Corbetti caldera through the Shalla-Corbetti segment of the Wonji Fault Belt.

CONTENTS

List of Figures

CHAPTER ONE

1.1 LOCATION

The study area (Fig.1) is located in the central part of the Main Ethiopian Rift (MER) within 38°15' and 38°45' longitude and 7°15' & 7°45' latitude centered about Shalla caldera, located about 41Km southwest of the Ziway town. The present-day Lake Shalla is 28Km long and 15Km wide with a maximum-recorded water depth of 257m. It occupies not only the O'a caldera which is characterized by a 17Km-long-axis diameter but also a tectonic depression immediately west of the caldera belonging to the northern end of the Shalla-Corbetti segment (Mohr et al., 1980).

1.2 Objective of the Study

The main objectives of this M.Sc research are:

1. To compile all the previous gravity data in a standard format and make it readily available for interpretation work with particular emphasis on the assessment of possible geothermal resources.

2. To make a preliminary qualitative interpretation of the resulting gravity anomaly patterns in terms of variations in density and geologic structures.

3. To investigate the nature of the gravity anomalies.

This thesis is organized into six chapters. The first chapter is introduction to thesis. The second chapter discusses the previous geological and geophysical works of the study area. The third chapter addresses the theoretical basis of gravity study. In the fourth chapter gravity data reduction, computation of different gravity anomalies and assessment of error associated with point Bouguer gravity anomalies and fifth chapter, compilation of the different Bouguer anomaly maps and a qualitative description of the observed Bouguer anomalies is presented. The last chapter presents discussion, conclusion and recommendation out coming from the study.

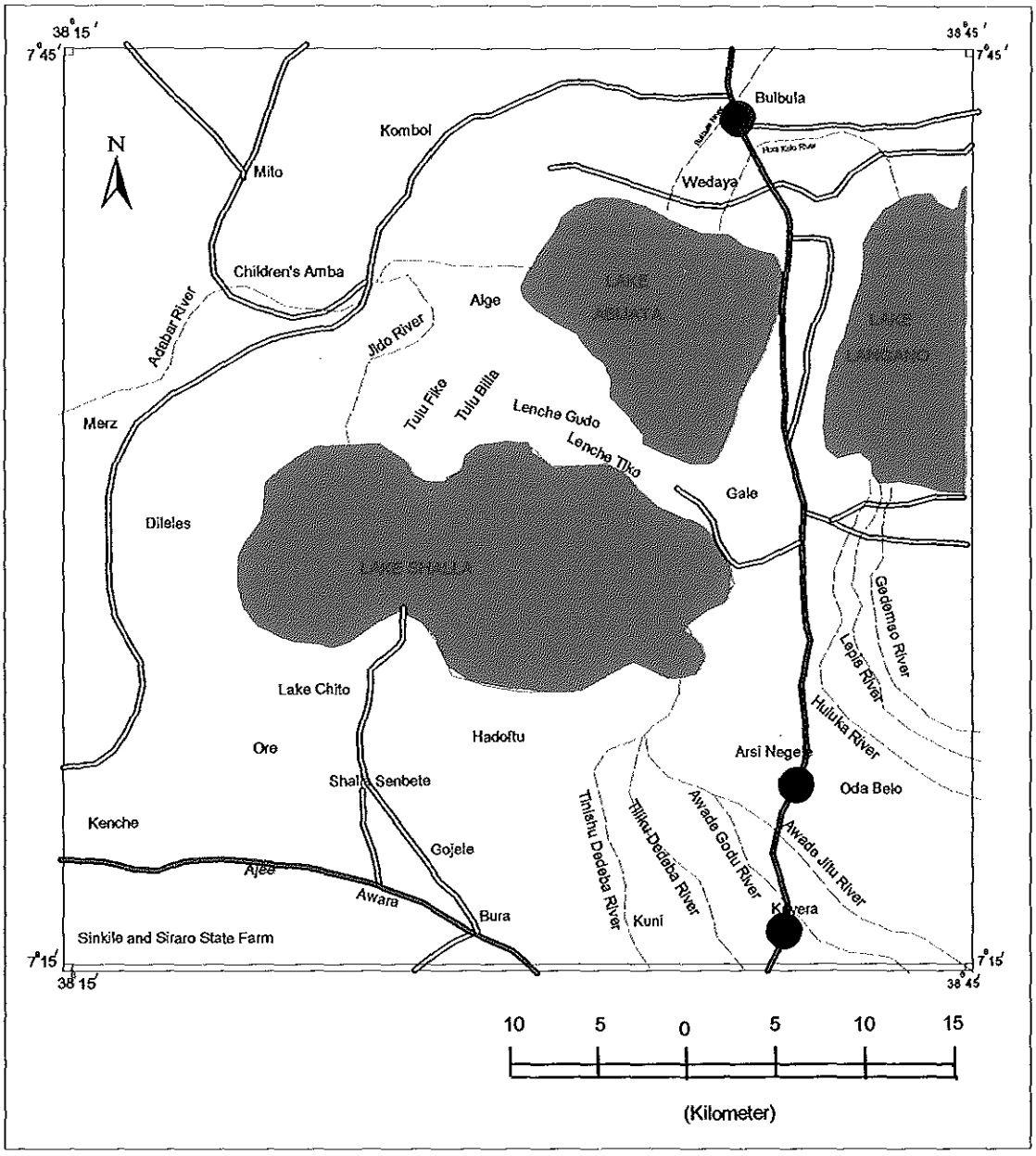

Fig 1. Location map of the study area.

CHAPTER 2

GEOLOGICAL SETTING OF THE STUDY AREA

2.1 General Introduction

The tectonic and volcanic activities that took place during the Cenozoic were significant in the making of the rift. At the beginning of the Mesozoic Era a shallow sea spread occurred over much of Ethiopia as a result of land subsidence. As the land continued to subside different types of deposits were accumulating in different places over the Precambrian basement rocks. Following the Mesozoic era there was extensive magmatism and faulting which modified the face of the East Africa. Faulting was accompanied by widespread volcanic activity. The region was subjected to two geologic events and other geologic processes of lesser magnitude. These geologic activities include uplifting of the Arabo-Ethiopian landmass and outpouring of huge quantity of magma, formation of the rift and Quartenary volcanism and deposition.

The Ethiopian rift system was formed by extensional tectonics (Mohr, 1967; Kazmin and Berhe, 1978). There is no universal agreement as to when the Ethiopian rift system begins to develop; according to Mohr (1967) the Afro-Arabian rift system is an expression of a tectonic zone of weakness in the lithosphere, which dates back to the Precambrian. However, the actual rifting process has commenced at the end of the Mesozoic or beginning of the Tertiary. Many authors have given different dates (Backer et al., 1972; Meyer et al., 1975; Kazmin, 1979; Kazmin et al., 1980). There is growing evidence that the development of the rift has been episodic rather than continuous (WoldeGabriel et al., 1990).

Volcanism in region of the southern and central sectors of the MER started as early as Eocene time with important basaltic eruptions, associated with an early stage of rifting characterised by uplift and faulting (WoldeGabriel et al., 1990,1991; Ebinger et al., 1993). From late Oligocene to early

Miocene times, the first major rifting within the MER resulted in a series of asymmetric half-grabens with alternating polarity (WoldeGabriel et al., 1990).

By late Miocene time, the eastern and western faulted margins of the rift had formed. Then, in late Miocene or early Pliocene time, evolution from alternating half-grabens to a full, symmetrical graben occurred. The present symmetrical rift was fully developed by 3.5 Ma, contemporary with a paroxysm of ignimbrite eruption when a 2000Km^3 ash-flow tuff (the Munesa crystal tuff) issued from large caldera located on the rift floor (WoldeGabriel, 1987). Since this period, major vertical displacement of up to 2 km has occurred in the central sector of the MER (WoldeGabriel et al., 1992).

Fragmentation of the rift floor formed the youngest structural deformation, largely concentrated within a narrow, 5-12 km wide belt of normal faults, known as the Wonji Fault Belt (Mohr et al., 1980; Lloyd, 1977). The Wonji Fault Belt (WFB) maintains a NNE orientation along the entire length of the MER and has been forced into en-echelon offsets in order to remain within the rift margin envelope (Mohr, 1980). This belt is regarded as a manifestation of incipient spreading centre. In Afar such structures are designated as axial ranges. The displacement lines of this fault belt are sites of maximum shallow crustal heating; this can be deduced from the present geothermal activity, the associated observed positive gravity anomalies and the quantities of volcanic products and their compositions.

In the central sector of the MER, the WFB is right laterally offset into four en echelon rift-axis segments, from north to south; Gedemsa-East Ziway, Ziway-Shalla, Shalla-Corbetti, and Duguna-Abaya segments (Mohr, 1960; 1967; Lloyd, 1977; Mohr et al., 1980; WoldeGabriel et al., 1990). Within the Ziway-Shalla region, the WFB is displaced from the median of the rift floor to become the marginal graben of the sector. Caldera-topped shield volcanoes occur at each WFB offset, the

Alutu Caldera between the Gadamsa-East Ziway-Shalla segments, the O'a caldera (presently occupied by Lake Shalla) between the Ziway-Shalla and Shalla-Corbetti segments, and the Corbetti Caldera at the south end of the Shalla-Corbetti segment (Mohr et al., 1980).

Major caldera subsidence occurred at O'a at a date close to 0.24 Ma with the accompanying emplacement of two ignimbritic flows: the "Strongly Welded Green" (greater than 70-m-thick) the "Weakly Welded Beige" (greater than 50-m-thick) Ignimbrites (Qi4 and Qi5 of Mohr et al., 1980).

2.2 Geology Of The Study Area

2.2.1 The O'a Caldera And The Lake Shalla Basin

The general shape of the depression occupied by Lake Shalla has also been modified by regional faulting (Fig. 2). Four main structural regions have been identified: the NNE-trending Eastern Shalla Fault system, the Northwest volcanic boundary, the Central Basin and the NNE-trending Southern Fault system (Tiercelin et al., 1997).

I. The Eastern Shalla Fault System: - This NNE-trending fault system belongs to the south end of the Ziway-Shalla WFB segment. It is connected to the north with the Katlo Horst through the Gale Horst that culminates at an altitude of 1714 m. To the north-northeast, the Eastern Shalla Fault system connects with the Mirga Graben extending south the Offshore Western Plateau of Lake Langano. Within this fault system, the major 15-Km-long, west-facing Roge Rafu Fault (RRF) with an apparent throw of 50 m corresponds to the tectonically rejuvenated wall of the O'a Caldera. Several N-NNE-trending fault segments presenting peculiar en relais fractures form RRF. A major 2-3-Km-long hydrothermal field occurs on the eastern shoreline near Rebo. The Eastern Shalla Fault system ends at about 7°20'N and is relayed to the west by the Shalla-Corbetti WFB segment.

II. The Northwest Shall Volcanic Boundary: - This boundary partly corresponds to the South-

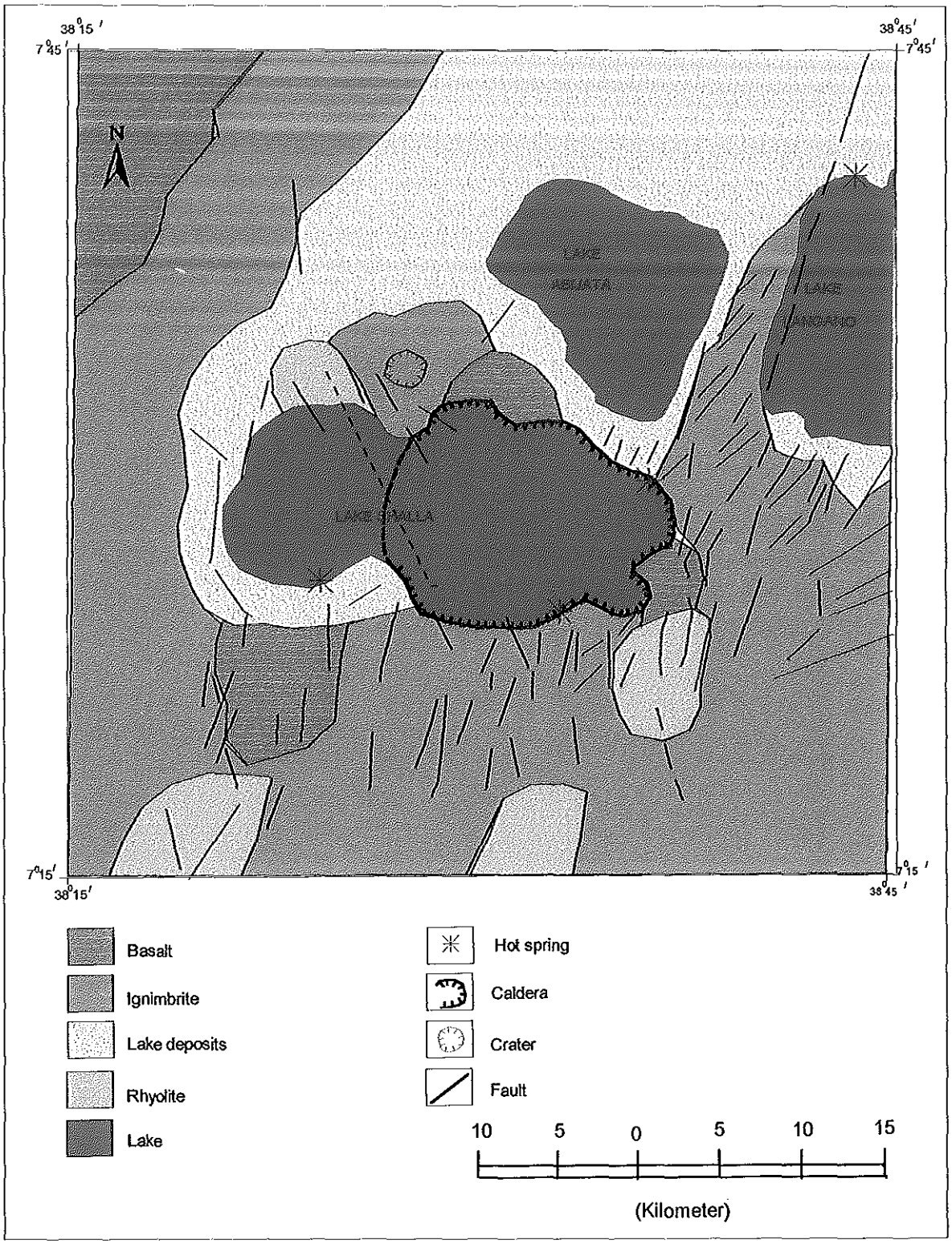

Fig 2. Geological map of the study area (after UNDP, 1973; Tenalem, 1998).

western Danga Volcanic Boundary of Lake Abijata Basin. It is formed by rhyolitic-type pumice, mainly air-fall pumice 5 to 40 m thick, related to the Tulu Fike cone that covers an area of 32 kilometres square, but also resulting from subaquitic eruptions. Tulu Fike is the only post-caldera parasitic centre identified at Shalla and is notable for being located well outside the main ring fault. ESE-trending faults between Tulu Fike and Tulu Billa suggest fault control on the late volcanic activity in this area (Mohr et al., 1980).

III. The Central Basin: - This corresponds to a very large, funnel-shaped caldera (estimated collapse volume of 120 Km^3) (Mohr et al., 1980) whose sides plunge steeply to depths exceeding 250 m, particularly along its southern shore (Baumann et al., 1975). This structure was produced by a volcanotectonic collapse of regional extension at a time close to 0.24 Ma. Sparse ESE-trending transverse faults with up throws of 5-30 m affect the eastern and western sides of the caldera.

IV. The Southern Shalla Fault System: - The southern shore of Lake Shalla is lined by precipitous cliffs more than 300m high, corresponding to the caldera walls. This morphology is intersected by the 12-Km-wide, submeridian fault system of the Shalla-Corbetti segment of the WFB. The western part of the lake corresponds to a NNE-trending elongated tectonic depression with a relatively flat and shallow floor (maximum water depth 50 m) belonging to the northern end of the Shalla-Corbetti segment (Baumann et al., 1975). Recent volcanic activity in this area is marked by basaltic flows, spatter cones, hyaloclastite rings at Hora Chitu and Mechefera, (Di Paola, 1972), and by several hot springs.

2.2.2 Structural Aspects Of Lake Abijata

The present-day Lake Abijata lies within a very flat depression characterised to the east by a gently faulted margin corresponding to the flank of the NNE-trending Katlo Horst, which separates Lake

Abijata from Lake Langano. The southern and western margins of the basin are essentially controlled by volcanic relieves partly belonging to the Shalla volcanic. To the north, a flat alluvial plain opens toward the Bulbul Plain and the Lake Ziway Basin. Three main structural regions have been identified within this basin: the East Abijata Border Escarpment, the Southwestern Danga Volcanic Boundary and the Main Basin.

I. The East Abijata Border Escarpment: - It corresponds to a several kilometres long, west-facing en relais fault system named the East Abijata Fault (EAF) which forms the eastern boundary of the Katlo Horst, and progressively disappears toward the north, below the Bulbula alluvial plain. With up to 20 m apparent throw, this fault is the part of the Ziway-Shalla WFB segment and affects the 0.23 Ma old "Strongly Welded Green" Ignimbrites, which blankets the rift floor. Comparatively to the well-expressed Western Langano Border Escarpment which forms the western boundary of the Katlo Horst, the East Abijata Fault is characterised by a deeply eroded morphology that possibly relate a breakdown in tectonic activity and subsidence in this area.

II. The Southwestern Danga Volcanic Boundary: - A large volcanic complex forms the southwestern of Lake Abijata, developing an isthmus of 70 m minimum height between Abijata and Shalla Lakes. The oldest outcropping volcanic within this area corresponds to the "Strongly welded Green" and the "Weakly Welded Beige" ignimbrites dated around 0.23-0.24 Ma (Mohr et al., 1980). Recent volcanic are represented by the fresh-looking Tulu-Billa (altitude1760) basaltic cinder cone dated at 0.18 Ma (Mohr et al., 1980). Scoriaceous basaltic flows of the Tulu Billa have been partially buried beneath sediments thought to be Holocene in age by Street (1979). Subaqueous volcanic described as "lacustrine guyots" form the Lencha Gudo (1750 m) and Lencha Tiko (1740 m) cones on the southern shore of Lake Abijata.

III. The Main Basin: - The very flat depression which corresponds to the Lake Abijata Main

Basin is bounded to the east by a small, deeply eroded escarpment which corresponds to the East Abijata Fault and disappears progressively toward the north, where the Abijata Main Basin joins the Bulbula alluvial plain. The origin of the Abijata Main Basin could be related to tectonic events and/or to major caldera development in the rift floor. The present blunted morphology of the East Abijata Fault may represent the final stage of development of a major fault system bounding to the half-graben to the east, consecutively to a breakdown in tectonic activity and basin subsidence in this area.

CHAPTER THREE

BASIC THEORY OF GRAVITATIONAL METHOD

3.1 Gravity and Gravimetry

Gravimetry is a method of measuring and modeling the gravity field of the earth (Torge, 1989). It is the measurement of gravity intensity, which is the magnitude of gravitational acceleration on or in the vicinity of the earth and other celestial bodies. The method of gravity survey in geophysics involves measurement, reduction, mapping and interpretation of gravity data (Dobrin, 1988).

3.2 Fundamental principle of gravity

The basis of the gravity survey method is Newton's law of gravitation, which states that the attraction force between two points masses m_1 and m_2, whose dimensions are small with respect to the distance r between them, is given by:

$$F= -G\, m_1\, m_2\, \hat{e}_r / r^2 \qquad (3.1)$$

where, r - is the distance between the masses

G - is the gravitational constant which is equal to $6.67 \times 10^{-11}\ m^3/kg\ s^2$

F - is the mutual force of attraction between m_2 and m_1.

$\hat{e}_r$ - is a unit vector whose direction is the line connecting the center of the two masses.

Since force is the product of mass and acceleration; the acceleration of m_2 is given by:

$$F= ma =- G\, m_1\, m_2\, \hat{e}_r / r^2 \qquad (3.2)$$

As a typical example, consider a mass m on the surface of the earth:

$$F= mg= G\, M_{ea}\, m / r^2\, \hat{e}_r$$

$$g = G\, M_{ea} / r^2\, \hat{e}_r \qquad (3.3)$$

g- is known as the gravity field or gravity field intensity or simply gravity. The unit of 'g' in geophysics is the Gal, in honor of Galileo Galilli.

$1 Gal = 1 cm / s^2$

3.3 Gravitational Acceleration External to the Rotationally Distorted Earth

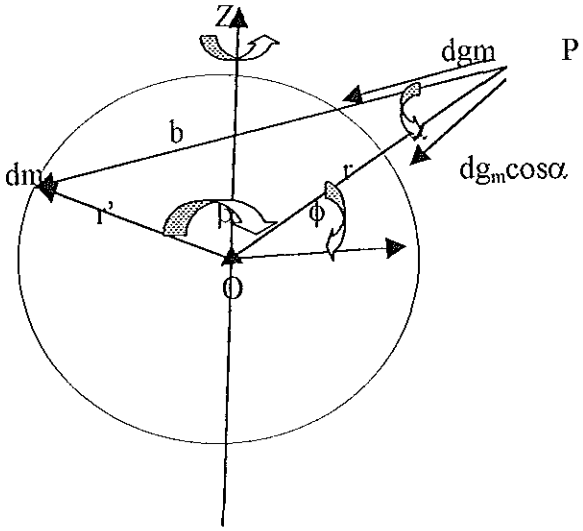

Fig. 3. Attraction, centrifugal force and gravity on spherical Earth

The gravitational acceleration at point P due to an element of mass dm is given by

$$dg_m = G\, dm/b^2 \qquad (3.4)$$

The component of this gravitational acceleration along the line from P to O is $G \cos\alpha\, dm/b^2$, the net radially inward gravitational acceleration at point P is found by integrating this expression over the entire mass distribution.

$$g_m = G \int(\cos\alpha/b^2)\, dm \qquad (3.5)$$

By using cosine law one can express $\cos\alpha$

$$\cos\alpha = (b^2 + r^2 - r'^2) / 2rb \qquad (3.6)$$

One can rewrite equation (3.5) for g_m by substituting expression (3.6) for $\cos\alpha$ with the result

$$g_m = G/2r^2 \int(r/b + r^3/ b^3\{1 - r'^2/ r^2\})\, dm \qquad (3.7)$$

The three distances appearing in the integrand of equation (3.7) r, r' and b are the sides of the triangle connecting O, P and dm in (Fig. 3). It turns out to be useful for carrying out integration to eliminate b from the integrand in terms of r, r' and the angle β. From the law of cosine one can write

$$b^2 = r^2 + r'^2 - 2rr' \cos\beta \qquad (3.8a)$$

by dividing both sides by r^2 the equation can be rearranged as

$$r/b = (1+ r'^2/r^2\, 2(r'/r)\cos\beta)^{1/2} \qquad (3.8b)$$

Upon substitution equation (3.8b) into equation (3.7) one obtains

$$g_m = G/2r^2 \int\{1+ r'^2/r^2 - 2(r'/r)\cos\beta\}^{-1/2}\,[1+\{1+r'^2/r^2-2(r'/r)\cos\beta\}^{-1}\{1-r'^2/r^2\}]dm \qquad (3.9)$$

An analytical evaluation of the integral in equation (3.9) is not possible. The integration is complicated because both r' and β vary with position of dm. However, the integration is tractable by approximating the integrand with a power series of r'/r. Using power series expansion and retaining the terms up to $(r'/r)^2$ only for point P outside the mass distribution $(r'/r)<1$.

$$(1+E)^{-1} = 1-E+E^2-.... \qquad \text{for } E<1 \qquad (3.10a)$$

Similarly

$$(1+ E)^{-1/2}=1- E/2+ 3E^2/8 -. . . \text{ for } E<1 \qquad 3.10b)$$

$$[1+r'^2/ r^2 -2r'/r\cos\beta]^{-1/2} = 1-r'^2/2r^2 + (r'/r)\cos\beta + 3/2\,(r'^2/ r^2)\cos^2\beta \qquad (3.10c)$$

$$[1+r'^2/r^2 - 2r'/r\cos\beta]^{-1} = 1-r'^2/2r^2 + 2(r'/r)\cos\beta + 4\,(r'^2/ r^2)\cos^2\beta \qquad (3.10d)$$

Using (3.10c) & (3.10d) in (3.9) to get:

$$g_m = G/ r^2\int dm + 2G/r^3 \int r' \cos\beta\, dm + 3G/ r^4 \int r'^2\,(1- (3/2)\sin^2\beta]\, dm \qquad (3.11)$$

The integration in equation (3.11) can be carried out in terms of well-known physical properties of mass distribution. The first term is just the integral of dm over the entire mass

distribution, the result is simply total mass M. The second term is the integral of r'cosβ over the mass distribution is a first moment of distribution which is by definition zero if the origin of the co-ordinate system is the centre of mass distribution, that is, $2G/r^3 \int r \cos\beta \, dm = 0$. Thus equation (3.11) becomes

$$g_m = GM/r^2 + 3G/r^4 \int r'^2 [1 - (3/2) \sin^2\beta] \, dm \qquad (3.12)$$

The integral appearing in equation (3.12) in terms of the moments of inertia of an axisymmetric body. Take C to be the moment of inertia of the body about the rotational axis or θ = 0 degrees; this moment of inertia is the integral over the entire mass distribution of dm times the square of the distance from dm to the rotational axis.

$$C = \int [X'^2 + y'^2] dm = \int r'^2 \sin^2\theta' [\cos^2\phi' + \sin^2\phi'] dm$$

$$C = \int r'^2 \sin^2 \theta' dm \qquad (3.13)$$

By using co-ordinates transformation

$$r'^2 = x^2 + y'^2 \qquad (3.14a)$$

$$x' = r' \sin\theta' \cos\phi' \qquad (3.14b)$$

$$y' = r' \sin\theta' \sin\phi' \qquad (3.14c)$$

$$z' = r' \cos\theta' \qquad (3.14d)$$

The moment of inertia about the x-axis, which is defined by $\theta = \pi/2$ and $\phi = \pi/2$

$$A = \int [y'^2 + z'^2] \, dm = \int r'^2 [\sin^2\theta' \sin^2\phi' + \cos^2\theta'] dm \qquad (3.15)$$

The moment of inertia about y-axis defined by $\theta = \pi/2$ and $\phi = \pi/2$, is

$$B = \int [x'^2 + z'^2] \, dm = \int r'^2 [\sin^2\theta' \cos^2\phi' + \cos^2\theta'] dm \qquad (3.16)$$

For a body that is axisymmetric about the z-axis or rotational axis A= B, the addition of equations (3.13), (3.15) and (3.16) together with the assumption of axisymmetry gives

$$A = B;\ A+B+C = 2\int r'^2\, dm = 2A+C \tag{3.17}$$

Equation (3.17) expresses the integral of r'^2 dm appearing in equation (3.12) in terms of moment of inertia of the body. To derive an expression for the integral of $r'^2 \sin^2\beta dm$, because of axial symmetry of the body there is no loss of generality in letting the line OP in (Fig.3) lies in the xz plane. With the help of equation (3.17), the required integral can be rewritten as

$$\int r'^2 \sin^2\beta\, dm = \int r'^2(1- \cos^2\beta)dm$$

$$= \int r'^2 dm - \int r'^2 \cos^2\beta\, dm = A+1/2C - \int r'^2 \cos^2\beta\, dm \tag{3.18}$$

The quantity $r'\cos\beta$ is the projection of r' along OP. This quantity expressed as can be

$$r'\cos\beta = x'\cos\phi + z'\sin\phi \tag{3.19}$$

where ϕ is the latitude or the angle between OP and the xy-plane. Note that y' has no projection onto OP, since OP is in the xz-plane. Equation (3.19) is used to write the integral of $r'^2\cos^2\beta$ in the form

$$\int r'^2 \cos^2\beta\, dm = \int x'^2 \cos^2\phi\, dm + \int 2x'z' \cos\phi \sin\phi\, dm + \int z'^2 \sin^2\phi\, dm \tag{3.20}$$

For an axial symmetric body:

$$\int (x'^2+y'^2)\, dm = 1/2C \tag{3.21}$$

The integral of z'^2 dm can be evaluated by using equation (3.13) & (3.17)

$$\int z'^2 dm = \int (x'^2 + y'^2 + z'^2)dm - \int (x'^2 + y'^2)dm$$

$$A+1/2C = \int (x'^2 + z'^2)\, dm + \int x'^2 dm = \int r'^2 dm$$

$$\int z'^2\, dm = A+1/2C - C = A-1/2C \tag{3.22}$$

With mass symmetry about the equatorial plane

$$\int x'\, z'\, dm = \int r'^2 \cos\theta' \sin\theta' \cos\phi\, dm = 0 \tag{3.23}$$

Substitution of equation (3.21) and (3.23) into equation (3.20) yields

$$\int r'^2 \cos^2\beta \, dm = 1/2C \cos^2\phi + (A - 1/2C)\sin^2\phi \quad (3.24)$$

When equation (3.18) and (3.24) are combined and by using the trigonometric identity

$$\sin^2\phi + \cos^2\phi = 1$$

$$\int r'^2 \sin^2\beta \, dm = A\cos^2\phi + C\sin^2\phi \quad (3.25)$$

The gravitational acceleration is finally obtained by substituting equations (3.17) and (3.25) into equation (3.12)

$$g_m = GM/r^2 - (3G/2r^4)(C - A)[3\sin^2\phi - 1] \quad (3.26)$$

is simplified form of Mac Cullagh's formula for an axis symmetric body. The moment of inertia about the rotational axis C is larger than the moment of inertia about an equatorial axis A because of the rotational flattening of the body. It is customary to write the difference in moment of inertia as a fraction of J_2 of Ma^2 i.e.,

$$C - A = J_2 Ma^2 \quad (3.27)$$

where a is the equatorial radius and J_2 is the polar moment of inertia. In terms of J_2, g_m can be expressed as

$$g_m = GM/r^2 - (3GMa^2J_2/2r^4)(3\sin^2\phi - 1) \quad (3.28)$$

The currently accepted values for a, GM and J_2 are: a = 6378.139km, GM=3.986005 $x10^{14}m^3s^{-2}$, and $J_2 = 1.0827 \times 10^{-3}$.

3.4 Centrifugal Acceleration and the Acceleration of Gravity

The force on a unit mass at the surface of the earth due to the rotation of the earth with angular velocity 'ω'is the centrifugal acceleration g_ω. It points out radially outward along a

line perpendicular to the rotation axis and passing through P refers to (Fig. 4) below. The following relations can be verified

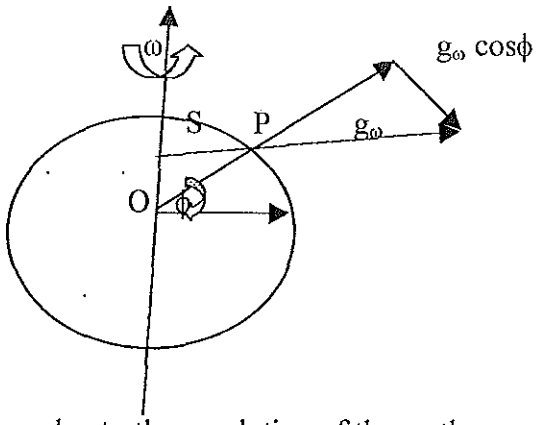

Fig. 4 The centrifugal force due to the revolution of the earth

$$g_\omega = \omega^2 S \tag{3.29}$$

where S is the perpendicular distance from P to the rotation axis. If r is a radial distance from P to the centre of the earth and ϕ is the latitude of point P

$$S = r\cos\phi \tag{3.30}$$

$$g_\omega = \omega^2 r\cos\phi \tag{3.31}$$

The gravitational and centrifugal acceleration of a mass at the earth's surface combined to yield the acceleration of gravity g. Since g_ω is very much less than g_m, it is appropriate to add the radial component of centrifugal acceleration to g_m to obtain g. As shown in (Fig. 4), the radial component of the centrifugal acceleration points radially outwards. In agreement with the our sign convection that inward-radial accelerations are positive, the radial component of the centrifugal acceleration is

$$g_r' = -\ g_\omega \cos\phi = -\ \omega^2 r\cos^2\phi \tag{3.32}$$

The acceleration of gravity g is the sum of g_m in equation (3.28) and g_r' due to the centrifugal acceleration, equation (3.32) with the result

$$g = g_m - g_r$$

$$g = GM/r^2 - (3GMa^2J_2/2\,r^4)\,(3\sin^2\phi - 1) - \omega^2\, r\cos^2\phi \qquad (3.33)$$

Equation (3.33) gives the radially inward acceleration of gravity for a point located on the surface of the model earth at the latitude ϕ and distance r from the centre of mass.

3.5 The Gravitational Potential and the Geoid

The gravitational potential V is the potential energy of m divided by its mass. Since g_m is a conservative field, it can be derived from V as

$g_m = \nabla V$ and Curl $g_m = 0$

$$V=\int_r^{\infty} g_m.dr' = -GM/r + (3GMa^2J_2/2r^3)(3\sin^2\phi - 1) \qquad (3.34)$$

The first term in the above equation is the gravitational potential of a point mass. It is also the gravitational potential outside a spherical symmetric mass distribution. The second term is the effect on the potential of the earth model' s rotationally induced oblatness. A gravitational equi-potential surface is a surface on which V is a constant.The gravity potential U accounts for both mass gravitation and rotation of the model earth.

$$U(r,\phi)=-\int_{\infty}^{r} g.dr' = -GM/r + (Gma^2J_2/2r^3)(3\sin^2\phi - 1) - 1/2\,\omega^2r^2\cos^2\phi \qquad (3.35)$$

A gravity equipotential is a surface on which U is a constant. Within a few meters, the surface defines an equipotential surface Geoid. An expression for the geoid surface that is consistent with the second order expansion of the gravity potential in the equation (3.35) can be obtained as follows

U at the equator - ($\phi = 0°$, r = a)

$$U_o = -GM/a + (Gma^2J_2/2a^3)(3\sin^2\phi - 1) - 1/2\,\omega^2 a^2\cos^2 0.$$

$$U_o = -GM/a\,[1 + 1/2\,J_2] - 1/2\,\omega^2 a^2 \qquad (3.36)$$

The value of the surface gravitational potential at the poles must also be U_o, since the surface of the model earth is defined to be an equipotential surface. Here r=b and $\phi = -\pi/2$

$U_o = -GM/ b +(Gma^2J_2 / 2b^3)(3\sin^2 90 - 1) -1/2\ \omega^2 b^2 \cos^2 90.$

$U_o = -GM/ b\ [1- (a/b)^2 J_2]$ (3.37)

The flattening (ellipcity) of the Geoid is defined by

$f = \frac{\text{Equatorial radius - Polar radius}}{\text{Equatorial radius}}$

$f = (a - b)/ a$ (3.38)

As expressed above;

U_o at the equator = U_o at the poles.

$-GM /a\ [1 + 1/2\ J_2] -1/2\ \omega^2 a^2 = -GM / b\ [1- (a/b)^2 J_2$ (3.39)

multiplying through out by - a/ GM gives

$1+1/2J_2+\omega^2 a^3/ 2GM = a/b(1-J_2(a/b)^2)$ (3.40)

Substituting b = a (1 -f) and neglect quadratic and higher order terms in f and J_2

(since $f<<1$ and $J_2<< 1$) the final expression for f can be obtained as follows

$f = 3/2J_2 +\omega^2a^3/ 2GM$ (3.41)

The shape of the model geoid is nearly that of a spherical surface; that is, if r_o is the distance tothe geoid then

$r_o \approx a(1- \varepsilon)$ (3.42)

where eccentricity is $\varepsilon<<1$. By setting $U=U_o$ and $r = r_o$ in the gravity potential equation and substituting the gravity potential at the equator for U_o and $r_o = a\ (1 -\varepsilon)$, and neglecting quadratic and higher order terms in f, J_2, $a^3\omega^2/GM$, and ε one obtains

$\varepsilon = (3/2\ J2 + \omega^2a^3/ 2GM) \sin^2\phi$ (3.43)

$r_o = a(1- \varepsilon)= a(1-(3/2J_2 +a^3\omega^2/2GM)\sin^2\phi)$

$r_o = a\ (1-f\sin^2\phi)$ (3.44)

where $f = 3/2\ J_2 + a^3\omega^2/ 2GM$

By convention, the reference geoid is a spheroid (ellipsoid of revolution) defined in terms of the equatorial and polar radii by

$$(r_o \cos \phi)^2 / a^2 + (r_o \sin \phi)^2 / b^2 = 1 \qquad (3.45)$$

The eccentricity of the spheroid is given by

$$\varepsilon = (a^2 - b^2)^{1/2}/ a = (2f - f^2)^{1/2} \qquad (3.46)$$

Using $b = a (1 - f)$ in the spheroid equation and simplifying for r_o gives

$$r_o = a (1 + (2f - f^2) /(1- f)^2(\sin^2\phi))^{-1/2} \qquad (3.47)$$

If this equation is expanded in powers of f and if terms of quadratic and higher order in f are neglected, the result is in agreement with $r_o = a (1-f\sin^2\phi)$. With a = 6378.139km and f = 1/ 298.256 defining the reference geoid; the difference in elevation between the measured geoid and the reference geoid ΔN is refereed to as a geoid anomaly.

The anomaly in the potential of the gravity field measured on the reference geoid ΔU can be related directly to the geoid anomaly ΔN. The potential anomaly is defined by

$$\Delta U = Um_o - U_o \qquad (3.48)$$

where U_{mo} is the measured potential at the location of the reference geoid and U_o is the reference value of the potential defined by equation (3.36). The potential on the measured U_o, as shown in the (Fig.5). It can be seen from the figure that U_o, U_{mo} and ΔN are related by

$$U_o = Um_o + ((\partial U/\partial r)_{r=r_o})\Delta N \qquad (3.49)$$

since $(\Delta N/a) << 1$. It will be recalled from the derivation of equation (3.35) that has been obtained the potential by integrating the acceleration of gravity. Therefore, the radial derivative of the potential in the equation (3.49) is the acceleration of gravity on the reference

geoid. To the required accuracy one can write

$$(\partial U/\partial r)_{r=ro} = g_o \qquad (3.50)$$

where g_o is the refence acceleration of gravity. Just as the measured potential on the refence geoid differs from U_o, the measured acceleration of gravity on the reference geoid is differs from g_o. Substitutionof equations (3.49) and (3.50) into equation (3.48) gives

$$\Delta U = -g_o \Delta N \qquad (3.51)$$

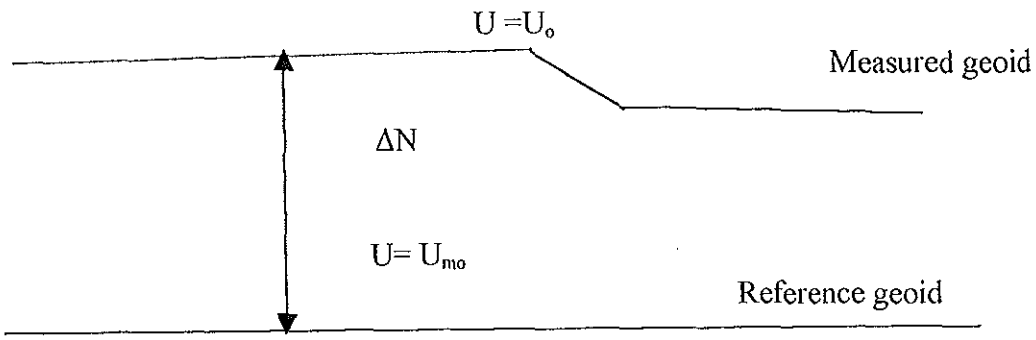

Fig. 5 Relationship of measured and reference geoid and geoid anomaly ΔN.

The reference acceleration of gravity on the reference geoid is found by substituting the expression for r_o given by equation (3.44) and (3.33) and simplifying the result by neglecting quadratic and higher-order terms in J_2, $a^3 \omega^2/GM$. One finds

$$g_o = GM/ a^2 (1 + 3/2\, J_2 \cos^2\phi) + a\omega^2 (\sin^2\phi - \cos^2\phi) \qquad (3.52)$$

To provide a standard reference acceleration of gravity against which gravity anomalies are measured, it is necessary to retain higher order terms in equation (3.52). Gravity anomalies are the differences between measured values of g on the reference geoid and g_o. By international agreements in 1967 the reference gravity field was defined to be

$$g_o = 978031.846[1+0.0052789\sin^2\phi - 0.000005\, \sin^2 2\phi] \text{ mGal} \qquad (3.53)$$

with g_o in ms^{-2}. This is the IGRS 1967 (International Geophysics Reference System) formula to calculate the theoretical gravity as a function of latitude (ϕ).

CHAPTER FOUR

REDUCTION OF GRAVIMETRIC DATA

4.1 Introduction

To produce the necessary information for the preparation of the final Bouguer gravity map, the following essential data must be determined at each observation point: relative gravity difference from one or more references or base stations, relative elevation for making the elevation correction and relative position for making latitude corrections and for mapping the final results. After the instruments determine the value of gravity, the following corrections are made: Free air correction, Bouguer correction, Terrain (topographic) correction, Latitude correction and Drift correction.

I. Latitude Corrections: - If the earth were a homogenous non-rotating sphere with the same vertical gradient everywhere, apart from local near surface density variations due to geological structures, and if it were a perfectly smooth surface, then clearly all gravity variations over the surface would be caused by geological structure. But this is not so. Because of the flattening, the poles are nearer to the center of mass than the equator, so the gravity increases with increasing in latitude. The variation of gravity with latitude over the surface of an ellipsoid earth can be expressed using the theoretical gravity formula (IGRS1967). The latitude correction δg_L is obtained by differentiating the theoretical gravity formula and is added to g as one moves towards the equator, i.e.

$$\delta g_L / \delta s = (1/R)\, \delta g_\phi / \delta \phi = 0.811 \sin 2\phi \text{ mGal} \qquad (4.1)$$

Where R = 6371km is the radius of the earth, and $\Delta s = R\delta\phi$ = N-S horizontal distance, and ϕ is the latitude angle (Telford, 1990).

I. Free Air Correction: -The free air correction is based on the fact that the attraction of the earth as a whole can be considered to be the same as if its mass were concentrated at its center. The free air correction takes into account the fact that each station is a different distance from the earth's center than the datum plane. If the elevation of a gravity meter is changed, its distance from the center of the earth changes by the same amount. The inverse-square law enables one to predict how much the acceleration of gravity will change as a result. Most stations are above sea level; the force of gravity becomes progressively less as the altitude becomes greater. So it is necessary to correct for changes in elevation between stations to reduce observations to a datum surface (Tsuboi, 1983). The correction is obtained by differentiating the scalar equation for a spherical earth

$$g = GM/ R^2 \qquad (4.2)$$

The gravity at a point located at a height h above the geoid is (Tsuboi, 1983)

$$g_h = GM/ (R+h)^2 = GM/ \{R^2(1+ h/R)^2 \}$$

$$= \{GM/ R^2\}(1+ h/R)^{-2} \qquad (4.3)$$

Applying the Binomial expansion for the term $(1+h/R)^{-2}$ and ignoring higher order terms and taking only the first two terms gives

$$g_h = \{GM/ R^2\}(1 - 2h/R) \qquad (4.4)$$

The free air correction is therefore given by

$$\delta g_{FA} = g - g_h = 2gh / R = 0.3086 mGal / m \qquad (4.5)$$

Note that the free air correction is added to the gravity reading when the station is above the geoid and subtracted when below it.

III. Bouguer Correction:- Rock masses between the station and sea-level increase the value of gravity; the amount being proportional to the altitude of the station and the density of the rocks between the station and sea-level. The Bouguer correction accounts for the attraction of the excess material between the station and the datum plane, which was ignored in free air correction. If the station were centrally located on a plateau of large horizontal extent and uniform thickness and density of gravity readings would be increased by the effect of this slab between the station and the datum plane. It is the correction for the attraction as approximated by considering the material as an infinite horizontal slab. The gravity attraction for a point on the surface of a slab obtained by calculating the effect of an infinite disk is given

$$\delta g_B = 2\pi G p h \qquad (4.6)$$

where h is the height of the gravity station above the geoid and G is the gravitational constant and p is the density. For mean crustal density ($p=2.67$ gm/cm^3) and h in meters, the Bouguer correction reduces to

$$\delta g_B = 0.1119h \text{ mGals/m} \qquad (4.7)$$

The Bouguer correction (reduction) is applied in opposite sense to the free air correction, i.e., it is subtracted when the station is above the geoid and vice-versa.

4.2 Computation of the Different Gravity Anomalies

Any local deviation of gravity from a more regular or smooth trend, which is defined by a group of several to many stations is an anomaly. Such anomalies are usually the primary data from which a geological interpretation of their source is attempted. In the geodetic sense, the anomaly is a single numerical value for any individual observation and is the difference of the observed value from a theoretical or calculated value based on certain assumptions about the form of the gravity field over the earth as a whole.

I. Free Air Anomaly: - Only the effect of elevation of a station from the geoid is considered by the free air anomaly. Here the attraction of materials between the elevation and the sea level (the geoid) will not be taken into account and that is why it is called the free-air. Thus, this free air anomaly is given by

$$\Delta g_{FA} = g_{obs} + 0.3086h - g_o \quad (4.8)$$

where g_{obs} is the observed gravity, g_ϕ is the theoretical gravity and h is the elevation.

II. Bouguer Anomaly: -The Bouguer anomaly is the difference between the measured value at the point of observation and the theoretical value calculated for that elevation or water depth, by considering a Bouguer slab of appropriate density for the effect of earth's material between the geoid and the station. The Bouguer anomaly calculated by ignoring topographic effects is known as simple Bouguer anomaly.

$$S.B.A. = g_{ob}s + 0.3086h - 0.1119h - g_o \quad (4.9)$$

When all corrections, the free-air, Bouguer, together with the terrain correction are applied to the observed gravity, the resulting anomaly obtained by subtracting the standard theoretical gravity at the given latitude is called the Complete Bouguer Anomaly (C.B.A) and is given by

$$\Delta g_B = g_{obs} + 0.3086h - 0.1119h + \delta g - g_o \quad (4.10)$$

4.3 Assessment of Errors in the Gravity Anomalies

The error that appears in the Bouguer Anomaly should be assessed before trying to compile gravity anomaly maps and begin to interpret gravity anomalies for the following reasons:

If it is not quantified and its magnitude is determined, the error can be interpreted as gravity anomaly and a false judgment can be arrived.

Error on Bouguer Gravity anomaly arises from: the precision in determining the geodetic latitude σ_ϕ, the precision in determining the elevation of the station σ_h, the reduction density σ_ρ, the reading

of the observed gravity value σ_g, the normal gravity value σ and instrument's accuracy.

The error involved in the point Bouguer anomalies can be expressed in its implicit functional form

$$\Delta g = \Delta g(g,h,\rho,\phi) \qquad (4.11)$$

The differential of equation (4.11) is used to compute the standard error due to the random errors ($\delta_{\Delta g}$)

$$d\Delta g = \delta_{\Delta g} = (\partial\Delta g/\partial g)dg+(\partial\Delta g/\partial h)dh+(\partial\Delta g/\partial\rho)d\rho+(\partial\Delta g/\partial\phi)d\phi \qquad (4.12)$$

The variance $\delta^2_{\Delta g}$ can be computed from the law of propagation of errors for uncorrelated observations according to

$$(\delta_{\Delta g})^2 = (\sigma_g)^2+(\partial\Delta g/\partial h)^2(\sigma_h)^2+(\partial\Delta g/\partial\rho)^2(\sigma_\rho)^2+(\partial\Delta g/\partial\phi)^2(\sigma_\phi)^2 \qquad (4.13)$$

The overall mean square error accuracy $\sigma_{\Delta g}$ of the point Bouguer gravity anomalies is defined by

$$\sigma^2_{\Delta g} = \delta^2_{\Delta g} + s^2_{\Delta g}$$

$$= (\sigma_g)^2+(\partial\Delta g/\partial h)^2(\sigma_h)^2+(\partial\Delta g/\partial\rho)^2(\sigma_\rho)^2+(\partial\Delta g/\partial\phi)^2(\sigma_\phi)^2+s^2_{\Delta}g \qquad (4.14)$$

where $\delta_{\Delta g}$ is the standard error (due to random errors) and $s_{\Delta g}$ is the systematic error (bias) of the gravity anomalies.

The individual contributions to the standard error, $\delta_{\Delta g}$, due to the random errors that occur naturally in the process of measuring the relative point gravity values, point elevations, point geodetic latitudes of the gravity stations and density of the topographic masses can be evaluated. The partial derivatives on the right hand side of equation (4.12) above are independently evaluated upon substitution of Δg by the Bouguer anomaly formula,

$$\Delta g_B = g_{obs} + 0.3086h - 0.04191\rho h - g_o.$$

I) The measurement precision σ_g (observational error) of the observed relative gravity value is evaluated by using the first partial derivative of Equation (4.12)

$$(\partial\Delta g/\partial g)dg = (dg/dg)dg = dg = \sigma_g \quad (4.15)$$

The measurement precision, σ_g, is obtained by computing the internal variance of the 12 independent observations made at the 4 gravity check points

$$\sigma^2_g = \{(\Sigma S_1(vv) + \Sigma S_2(vv) + \Sigma S_3(vv) + \Sigma S_4(vv)\}/(n-s) \quad (4.16)$$

where n is the total number of independent observations, S_1, S_2, S_3 and S_4 are the number of gravity check points, and v's are residuals for the individual observations at each check point and y_1, y_2, y_3, and y_4 are the mean values of each observation in Table 1. Table of observed relative gravity values (mGal) for computing the internal variance of 12 independent observations taken at 4 check points.

Gravity check point (S)	Observed relative gravity (Y)	Residual v	vv	Summation $\Sigma_{Sn}(vv)$	
S1:	1015.90	1015.92	-0.02	0.0004	$\Sigma_{s1}(vv) = 0.0078$
	1015.99	1015.92	0.07	0.0049	
	1015.87	1015.92	-0.05	0.0025	
	Mean	$y_1 = 1015.92$			
S2:	0994.99	0994.92	0.07	0.0049	$\Sigma_{s2}(vv) = 0.0083$
	0994.89	0994.92	-0.03	0.0009	
	0994.87	0994.92	-0.05	0.0025	
	Mean	$y_2 = 0994.92$			
S3:	1030.67	1030.69	-0.02	0.0004	$\Sigma_{s3}(vv) = 0.0078$
	1030.76	1030.69	0.07	0.0049	
	1030.64	1030.69	-0.05	0.0025	
	Mean	$y_3 = 1030.69$			
S4:	1027.71	1027.74	-0.03	0.0009	$\Sigma_{s4}(vv) = 0.0083$
	1027.81	1027.74	0.07	0.0049	
	1027.69	1027.74	-0.05	0.0025	
	Mean	$y_4 = 1027.74$			

Findings of this investigation indicate that the gravimeter has a measurement precision computed using Equation (4.18) as,

$\sigma_g = \pm [(0.0078 + 0.0083 + 0.0078 + 0.0083)/(12-4)]^{½}$

$= \pm 0.06$ mGal

$\sigma_g = \pm 0.06$ mGal is, therefore, the computed observation error estimate (the overall reproducibility of the gravimeter readings) that one may encounter when taking readings with this gravimeter.

II) The second Partial derivative of equation (4.14) results in,

$(\partial\Delta g/\partial h)dh = d/dh(0.3086h-0.04191\rho h)dh$ (4.17)

By making use of the adopted reduction density, $\rho = 2.67$ g/cm^3 and the precision in the elevation determination, $\sigma_h = \pm 10$m, reported, the error introduced in the computed Bouguer anomalies due to elevation error is

$(0.3086-0.04191 \times 2.67)\sigma_h = \pm 1.97$ mGal. (4.18)

III) The third partial derivative of equation (4.16) results in

$(\partial\Delta g/\partial\rho)d\rho = d/d\rho(0.04191\rho h)d\rho$ (4.19)

Supposing that one wants to achieve a reduction precision of 0.2 mGal in the Bouguer reduction using the Bouguer plate gravity formula given by

$g_{BP} = 2\pi G\rho h = 0.04191\rho h$ (4.20)

The precision of density determination, which is required for the computation of Bouguer anomalies follows as,

$\sigma_\rho = d\rho = (1/0.04191h)dg_{BP}$ (4.21)

For the mean elevation, h =1682.902 meters, of the gravity stations considered within the limits of the study area in the application of the reduction density, $\rho = 2.67$ g/cm^3, the precision of adopting this density value would amount to,

$\sigma_\rho = (1/0.04191 \times 1682.902) \times 0.2 = 0.0028$ g/cm^3 (4.22)

The error introduced in the computation of the point Bouguer anomalies due to density error is

therefore computed as,

$(\partial\Delta g/\partial\rho)d\rho = (0.04191 \times 1682.9)\sigma_\rho = \pm 0.20$ mGal (4.23)

IV) The last partial derivative of equation (4.16) results in,

$(\partial\Delta g/\partial\phi)d\phi = 1/R(\partial g_o/\partial\phi)d\phi$ (4.24)

By differentiating the expression for the normal gravity given by equation (4.11), with respect to ϕ and letting R = 6371229m (mean earth's radius), the rate of change of the normal gravity with latitude is estimated by

$1/R(\partial g_o/\partial\phi) = 0.813 \sin 2\phi$ mGal/km (4.25)

For the mean latitude, $\phi \leq 7.5°$ of the study area, the variation in the normal gravity is about 0.00021 mGal for each meter traveled in a N-S direction. For the precision estimate within the radius of $R\sigma_\phi = \pm 200$ m, in the determination of the latitude (UTM coordinates) of the gravity stations scaled from 1:250,000 and 1:50,000 topomaps, the error estimate in the normal gravity reduction for the computation of the Bouguer anomalies amounts to

$1/R(\partial g_o/\partial\phi)R\sigma_\phi = 0.042$ mGal (for $\phi \leq 7.5°$) (4.26)

is computed upon substitution of the values evaluated using Equations. (4.16), (4.18), (4.23) & (4.26) for each term on the right hand side of Equation (4.14) and amounts to

$\sigma_{\Delta g} = \pm [(0.06)^2 + (1.97)^2 + (0.20)^2 + (0.042)^2 + 2^2]^{1/2} = \pm 2.82$ mGal

Since a systematic error, $s_{\Delta g} = 2$ mGal is introduced in the survey process due to neglect of terrain correction, the overall mean square error, $\sigma_{\Delta gB}$, of the point Bouguer anomalies computed using equation (4.11) amounts to the effect of the random errors and the systematic error and is estimated at $\pm$ 2.82 mGal.

CHAPTER FIVE

ACQUISITION, PROCESSING AND INTERPRETATION OF THE GRAVIMETRIC DATA

5.1 Acquisitions and Processing of the Gravimetric Data

The data used for the gravity methods employed under this study are obtained from two sources: the Geophysical Observatory of Addis Ababa University from gravity data compiled by Dr. Abera Alemu and the Geological Survey of Ethiopia (GSE). A total number of 1041 gravity stations are obtained from the GSE upon a research co-operation agreement between the AAU and GSE.

The theoretical gravity, g_o, at latitude ϕ, has been calculated from the 1967 gravity formula (Geodetic Reference system 1967; Moritz, 1971). A total of 1041 observations are therefore treated under this MSc. research by a homogeneous reference to the IGSN71 datum. The elevations and positions (latitude and longitude) of the gravity stations that were observed in the Shala Caldera and its surroundings were determined with altimeters, barometers and 1:50,000 scale topographic grid maps and are reported to have an error of ± 10 meters, and their positions were scaled from 1:50,000 scale topographic maps and are reported to have an accuracy of ±5 meters.

Then free-air and Bouguer corrections were applied according to the theoretical schemes that have been discussed in the previous sections. A uniform reduction density of 2.67 gm/cc is used to compute the Bouguer anomalies. The point free air and Bouguer anomalies were computed in accordance with the standard formula treated in the theoretical part (Sections 4.1 and 4.3) respectively. The computed Bouguer anomaly corresponds to the simple Bouguer anomaly, as terrain correction is not taken into consideration.

Furthermore, the separation of the regional effect from the Bouguer anomaly was performed using

the GEOSOFT mapping software based on the trend surface of the regional gravity anomaly approximated using a polynomial surface fitting of degree 3. The corresponding residual anomalies were then obtained, and using the same square grid interpolation with a grid cell size of 0.25, the regional anomaly map (Fig. 9) and residual anomaly map (Fig. 10) are produced. Preliminary qualitative interpretation of these maps has been made using as a constraint, the geological map (Fig. 2) of the study area and the results of previous geophysical and geological surveys discussed in chapter two.

5.2 Descriptions and Interpretation of the Different Anomaly Maps of the Study Area

The first step in the interpretation of a geophysical survey data is compilation of anomaly maps of the area considered. The computed anomaly values are reported as elevation map (Fig. 6), free-air anomaly map (Fig. 7), Bouguer anomaly map (Fig. 8), Bouguer residual anomaly map (Fig. 9), Bouguer regional anomaly map (Fig. 10) by plotting them on 1:250,000 scale map of the study area. The contouring is made in 5mGal interval for all gravity anomaly maps contour interval (CI) isoanomaly curves. The task is performed using the standard gravity mapping and processing software.

5.2.1 Free-air Anomaly and Elevation Map

The free air anomaly map is produced with a contour interval of 5 mGal and the elevation map of the same scale with a contour interval of 50 m to observe the relation of the free-air anomaly to the elevation map. There is a close correlation between the pattern of elevation map (Fig. 6) and free air anomaly map (Fig. 7) of the study area. For instance, the maximum values of elevation and free-air anomaly maps are found at the NW, SE and SW part of the study area. The minimum values of elevation and free-air anomaly are found over the lake Abijata and Langano, at the eastern, southeastern and southwestern coast of lake Shalla. On the other hand there is a maximum value of

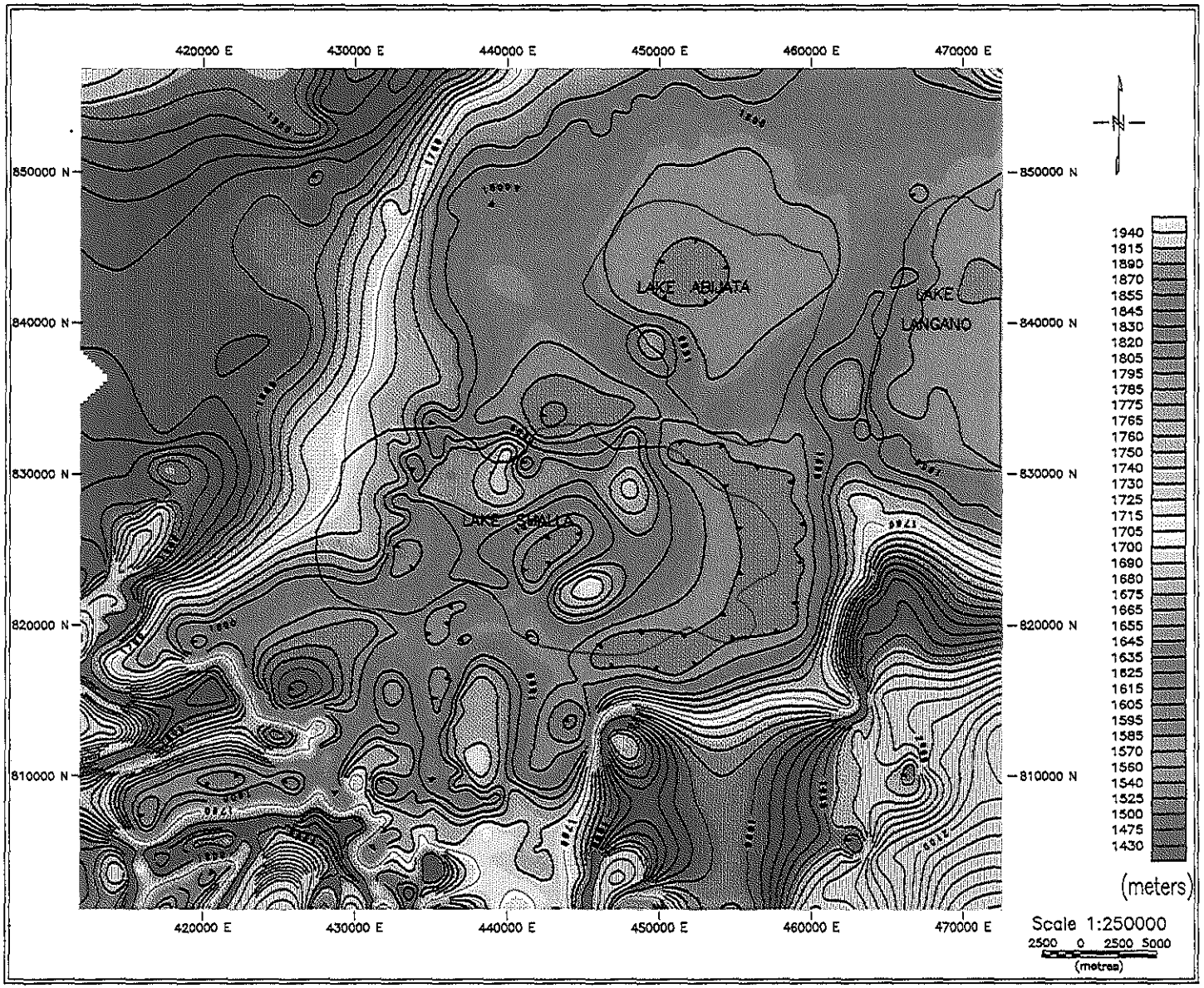

Fig 6. Topographic map of Shalla caldera and its environs.

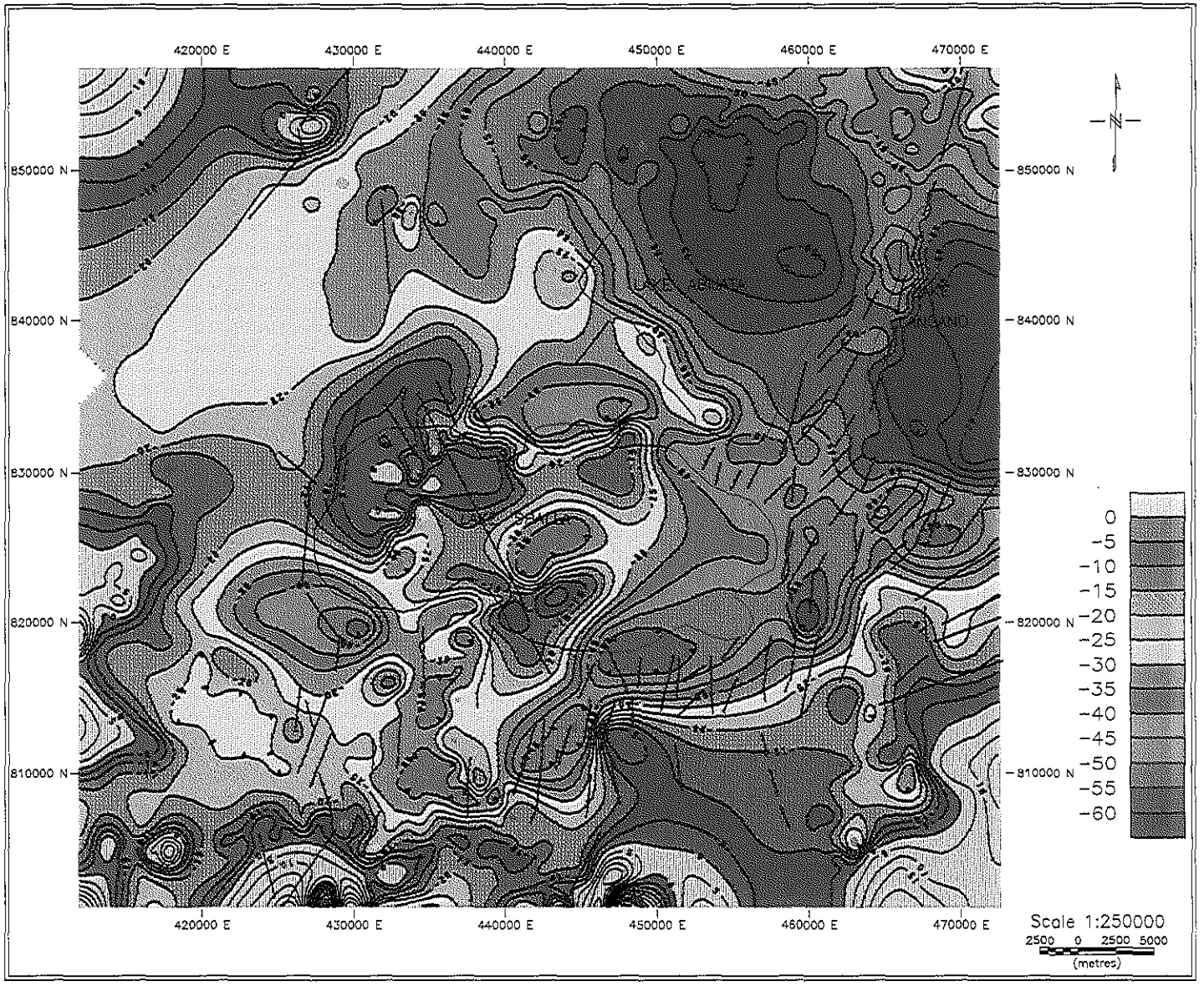

Fig 7. Free-air anomaly map of Shalla caldera and its environs.

free-air anomaly at the central part of the study area where the value of the elevation map is minimum. However, an overall correlation cannot be obtained between the anomalies and the subsurface geological and structural features.

Any free air anomaly map from land observations will show a strong correlation with local topography, i.e., the fee air anomaly is greater than zero for uplifted topography. Due to strong correlation with height, maps of free air anomalies are not well suited for local gravity field displays on land. The free air anomaly in the study area varies from a minimum value of -70 mGal in the southern part of Lake Langano to a maximum value of 15 mGal in the southeastern corner, which is the continuation of the eastern plateau. In the central, southern, SW and NW part of the study area the pattern of free air anomaly is similar to the Bouguer anomaly of (Fig. 8), i.e., both have positive values. The northern, NE, western part of Lake Langano and the eastern shore of Lake Shala are clearly indicated by the negative free air anomalies and most of these area corresponds to the lowland.

5.2.2 Bouguer Anomaly Map

On a continental platform the Bouguer anomaly is less than zero and strongly negative on high mountains. This is due to a mass deficit that exists beneath the continents causing the negative Bouguer anomaly. Topographic masses shifted to a level below the geoid are not resting on homogeneous crust of constant density or they are not superimposed on homogeneous crust of constant density. Therefore, such gravity anomalies are thought to be caused by a change in mass distribution underneath the observation points. These mass distributions could be of shallow or deep origin. Shallow origin mass distributions are subsurface anomalous masses with lateral density variations. Subsurface anomalous masses give rise to negative or positive Bouguer anomalies depending upon their density contrast with respect to the mean crustal density (2.67gm/cm^3) used

in the Bouguer reduction. The lateral extent of Bouguer anomalies due to subsurface anomalous bodies is small as compared with those of Bouguer anomalies of deep origin anomalous bodies. In general the Bouguer anomalies on local scale is caused by the lateral variation in density of subsurface masses. On the other hand the non-homogeneous crust of variable density and thickness causes the anomaly on regional scale. On gravity map, the strike of the anomalous subsurface body is the direction of the elongation of the closed curves. High horizontal gradient indicates contacts between rock units of different densities. The steeper the gradient the shallower the contact between rock units having different densities.

The Bouguer anomaly map (Fig. 8) is generated with a contour interval of 5mgal. The intensity of the Bouguer anomaly field within the study area varies from a minimum of -240 mGal to maximum of -190mGal. Based on the continuity, extension, pattern, orientation and distribution of the different positive and negative gravity anomalies, the study area is designated by anomaly A, B, C and D in order to facilitate the description and interpretation of the Bouguer anomaly map.

Anomaly A

It includes the southern and southwestern part of the study area. This anomaly occurs at the location of the northward extension of the Corbetti caldera towards the Shala caldera at the southern part of the study area. There is an elongated posistive Bouguer anomaly extending from the SW corner up to the SW coast of Shalla caldera, which intersected the negative anomalies surrounding the southern and western coast of Shalla caldrea. There is a major positive anomaly oriented in the N-S between 450000E and 460000E. This may be ascribed to the high density intrusive related to volcanotectonic complex of the Shalla-Corbetti segment of the WFB. There are several circular and elongated negative anomalies which could be attributed to the rift volcanoes and maximum depth of lake sediments.

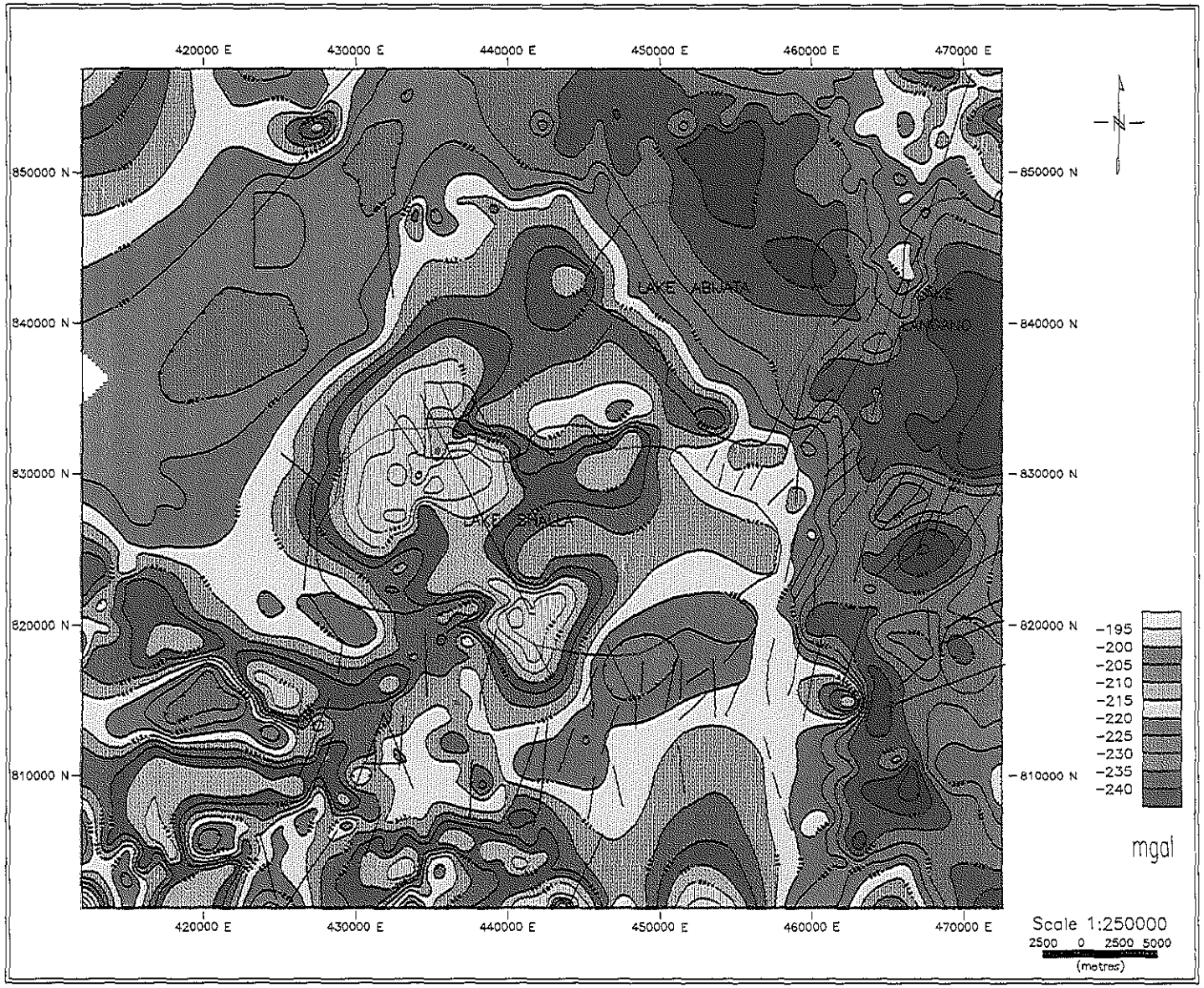

Fig 8. Bouguer anomaly map of Shalla caldera and its environs.

In the SW part of the study area there are elongated positive anomalies oriented approximately in the E-W direction, which are separated by the negative anomaly, oriented in the SW-NE direction. As clearly indicated on the Bouguer anomaly map the high horizontal gradients indicate the existence of contacts between rock units of different density in this area.

Hot ground and fumaroles that probably existed throughout the life of the Corbetti caldera's and persist to the present. They are mainly associated with the rhyolitic volcanism, but some hot ground areas beyond the northern rim of the caldera occur in close association with basalts. It is suggested that the Corbetti caldera volcanism is the probable heat source for all hydrothermal activity south of the Shalla caldera. In this area, the local geothermal manifestations are aligned along active faults and recent central volcanic complexes. Only fumarolic activity is associated with Corbetti volcanic centre (UN, 1973).

Anomaly B

It includes the Shalla caldera and the southern and northwestern coast of lake Abijata. In marked contrast with other lakes, Shalla is very deep and bounded by a steeply dipping caldera rim. Its longest axis is approximately normal to the strike of the regional faults, whereas all other lakes in the region are elongated in the NNE direction parallel to the rift axis. Lake Shalla occupied a major volcano-tectonic collapse caldera modified by subsequent regional faulting. The western lake floor is relatively flat and shallow, and bounded on the west by linear NNE faults downthrown east belonging to the northern end of the Shalla-Corbetti segment of the Wonji Fault Belt. It is suggested that this part of the lake occupies a graben; a similar structural environment for other tectonic lakes in the region. However, the fault blocks forming the eastern wall of the graben are breached on the east by the collapse of the western part of the elliptical Shalla basin.

There is broad major positive anomaly occurring at the western coast of the Shalla caldera and at

the location of the Northwest Shala volcanic boundary, which partly corresponds to the southwestern danaga volcanic boundary of Lake Abijata basin. This positive anomaly may be ascribed to the presence of high-density magmatic intrusions or the existence of buried caldera, which is the source of heatto the fumarolic activity. The oldest outcropping volcanic rocks within this area, i.e., the strongly welded green and the weakly welded biege ignimbrite, basaltic cider cones may contribute to this positive anomaly or this may be related to the intrusion and the recent volcanism in the Corebetti and O'a calderas. The small and elongated positive Bouguer anomaly located at the northeastern coast of Shalla caldera may be ascribed to the basaltic flows and rhyolitic intrusions. The negative anomaly at the northern coast of Shalla caldera may be caused by undifferentiated ignimbrite, interbedded air-fall tuff and pumiceous pyroclastic flows.

The relatively positive Bouguer anomaly in the southwestern and southern coast of lake Abijata is related to the causes of surface thermal features. Moreover, the alkaline lakes of Shalla and Abijata are hot. Abijata has higher surface temperature than Shalla (Tenalem, 1998). This may be related to its shallow depth and the thermal properties of the lake water and bottom sediments.

The western and southern coast of Shalla caldera is surrounded by negative Bouguer anomalies. At the Shalla caldera, there is a subsidiary circular depression close to the south-eastern coast, and another forming an embayment in the steep submerged western wall of the graben. This area is characterized by an elongated negative Bouguer gravity anomaly which intersects the wall of the Shalla caldera following the orientation pattern of the Shalla-Corbetti segment of the WFB that is NE-SW. Furthermore, this negative Bouguer anomaly corresponds to the large fault controlled hot springs found at the southeastern coast of Shalla caldera. The cause of this negative anomaly may be due to the steam fraction in the high-porosity reservoir rocks as well as to the lowered density

caused by thermal expansion. Therefore, this negative gravity anomaly corresponds to one of the sites of geothermal manifestations located at the southeastern coast of Shalla caldera.

There is a positive Bouguer gravity anomaly which extended from the southern coast of Shalla caldera and passing through the western part following the fracture emanating from the NW to SE coast of Shalla caldera. The site over which this anomaly occurs is marked by several hot springs and mini calderas like Chitu Haro craterd with hot waters. Therefore, this maximum value of positive Bouguer gravity corresponds to one of the sites of geothermal manifestations in the area.

Ignimbrites surrounding the Shalla caldera are intersected by numerous faults which commonly strike NNE and produce small horsts and grabens. These structures probably play an important role as conduit for groundwater inflow to the lake and hydrothermal activity of the Shalla caldera. The main inflow to the lake Shalla passes through the open faults and volcanic vent structures; diffuse flow in the fractured areas is probably very small. The possible sites of water inflow to the lake Shalla are from the southern side through SE-NW trending faults and from the northern and north-eastern side through the faults and vents intersecting the N-S trending faults that pass through lake Langano.

The eastern coast of Shalla caldera is surrounded by a negative anomaly approximately following the orientation pattern of N-S trending fault systems. The negative anomaly at the eastern part of lake Shalla belongs to the Eastern Shalla fault system which is connected to the north with the Eastern Abijata fault system and to the south with the Southern Shalla fault system. This negative anomaly is an integral part of the NNE-trending fault systems and belongs to the south end of the Ziway-Shalla WFB segment. A major 2-3-Km-long hydrothermal field occurs on the eastern coast of lake Shalla. This hydrothermal activity is related to the hot springs flowing to the lake through

regional faults that trend NNE and displace ignimbrites. There is a small circular positive gravity at the southeastern part of Shalla caldrea. This positive anomaly is caused by the rhyolitic intrusion.

Anomaly C

It includes eastern and southeastern part of Shalla caldera; northern, northeastern and eastern part of lake Abijata; and northern, western and southwestern part of lake Langano. This area is clearly indicated by the gravity low that extends from the northern to the southeastern part of the study area. To the north of Lake Abijata, a flat alluvial plain, which opens toward the Bulbula Plain and the Lake Ziway Basin, is indicated by gravity minima. These negative anomalies are oriented in a NW-SE and N-S direction. The ideas of southward migration of groundwater from lake Ziway and lower Katar catchment is supported by the existence of highly evaporated water in wells between Ziway and Abijata lakes, and the hot springs and thermal gradient wells of northern Langano (Tenalem, 1998).

Lake Abijata is indicated by the almost flat negative anomaly. The flatness of the anomaly may be due to the fact that the basement is closer to the surface in this area. So the density contrast of the overlying units is negligible and hence does not produce significant anomalies compared to the 2.67 gm/cm^3 mean crustal density used for the data reduction.

This type of strong and smooth negative anomaly is also found in the western and northern part of Lake Langano, eastern part of the Lake Abijata, which extended from the negative anomaly in the northern and northeastern part of Lake Abijata with the same amplitude of gravity minima -240 mGals. It is approximately found between 830000 N and 847000 N. This negative anomaly includes the Katlo horst which separates lake Abijata from lake Langano; West Langano fault and Eastern Abijata fault system which forms the eastern boundary of the Katlo horst and belongs to the south end extension of the Ziway-Shala segment of the WFB, the northern part of the study

area. The high gravity gradients indicate a shallow origin for this negative anomaly, which could be interpreted as due to low-density material of recent sediments of lacustrine deposits, siltstone, sandstone, and interbedded tuff, which are predominantly rhyolitic (Abera, 1983).

The positive anomaly located in the NE corner of the study area is the continuation of the Aluto caldera. This strong positive anomaly generated by the Aluto caldera could have influence or could have inhibited the effect of a deeper sedimentary basin extending further to the east. The asymmetrical and elliptical shape of the negative anomaly and its general submeridian trend suggest an east dipping, strongly asymmetric half-graben for the Abijata main basin. Another small volcanic centre and hot springs are clustered at the northern side of lake Langano in four localities: Oitu, Gesyer Island, Bole and Tuffa springs. The focus of the circular scarp of the centre is located on Geyser Island, which is a rhyolitic dome in the North Bay of Lake Langano. The Island has been interpreted as a rhyolitc intrusion (UN, 1973). The hottest spring in this locality is coincident with a gravity high.

There is another negative anomaly in the eastern and southeastern part of Shalla cadera; southern and southwestern part of lake Langano which extends up to the southeastern corner of the study area which is found between 800000 N and 830000 N. Most of this negative anomaly is an extension of the northern part of the study area.

The negative anomaly in the southern part of lake Langano and southeastern corner belongs to the eastern rift escarpment. At the southeastern corner of study there is another positive anomaly oriented in the N-S direction around the town of Kuyara. In general, the continuity of these negative anomalies from the northern to southeastern part of the study area indicates the presence of integral geologic structures responsible for the formation of these anomalies. The presence of continuity of faults and similar geologic structures are believed to provide the routes for the

migration of water, southward movement from the north, and northward migration from the lake Awassa basin, ultimately towards the lowest elevation where the three lakes (Shala, Abijata and Langano) are situated.

Anomaly D

It includes the western and NW part of the study area. A clear broad negative anomaly is found in the NW part of the study area. This negative anomaly is the part of Mt.Gurage that forms the western margin of the rift between 8°N and 8° 30'N. Principal faults appear which trend along the typical NNE-NE rift direction. This negative anomaly may be ascribed to undifferentiated ignimbrite, interbedded air-fall tuffs, pumiceous pyroclastic flows, basaltic cones and flows interbedded with lake deposits.

There is a positive anomaly in the NW corner of the study area in a region close to the Gedamotta caldera. This positive anomaly may be ascribed to the presence of high density intrusive or this anomaly is the result of high-density material such as trachyte, non-prophyritic obsidian, rhyoltic flows, domes and undifferentiated pyroclastics. The Gedamotta caldera is an early Pleistocene alkaline and pre-alkalne rhyolitic lava flow and bedded tuff located west of Ziway.

5.2.3 Bouguer Residual Anomaly Map.

The Bouguer residual anomaly map (Fig. 9) is produced with contour interval of 5mGal from the third order residual gravity values obtained by subtracting the regional anomaly from the Bouguer anomaly using trend surface analysis. The residual anomalies include anomalies of short-wavelength up to 33 Km depth. The local anomalies have short-wavelength, high amplitude and small lateral extent (perceptible over short distances) being caused by relatively small geologic features that are of interest in prospecting work. The residual gravity anomaly characterises the general pattern of

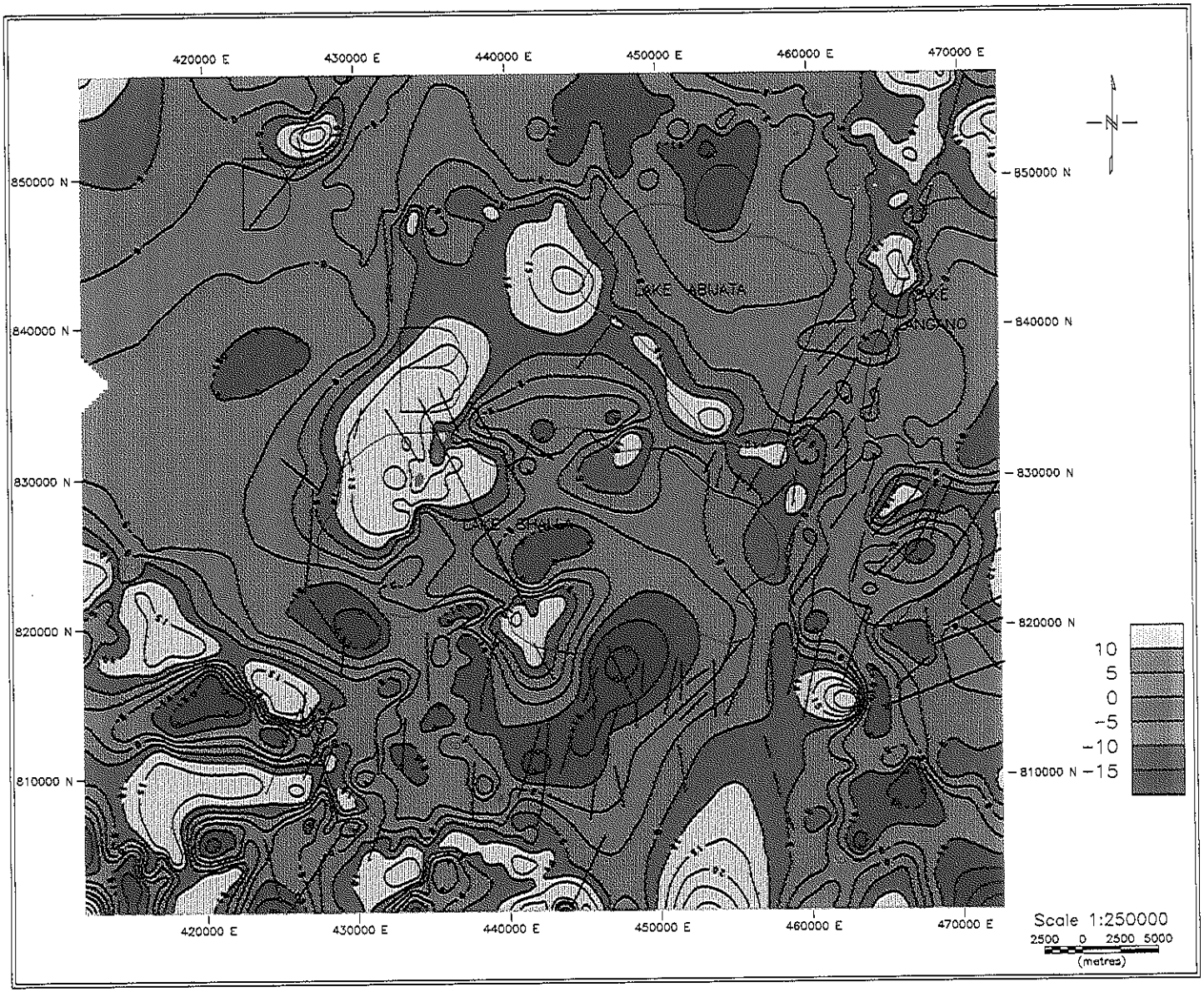

Fig 9. Bouguer residual anomaly map of Shalla caldera and its environs.

the Bouguer gravity map, but with small local anomalies are appearing after the removal of the regional. The local positive anomalies appear in the eastern coast of Shalla caldera, northwestern and northern coast of lake Langano and SE part of the study area. The intensity of residual gravity anomaly in the study area ranges from a maximum value of 15mGal to a minimum value of -10mGal. Similar to the Bouguer gravity anomaly, the distribution, pattern and location of the most prominent anomalies of the study areas revealed by the Bouguer residual anomaly map are designated by anomaly A, B, C and D to facilitate their description and interpretation (see Fig. 9).

Anomaly A

This anomaly includes the southern and southwestern part of the study area. Most of these areas are indicated by the major and subsidiary positive residual gravity anomalies. The major positive residual gravity anomalies located in the western part of the study area between 815000N and 828000N follow approximately the orientation pattern of W-E and changed NW-SE. In this area there is an elongated negative anomaly surrounded by the positive anomalies approximately between 813000N and 817000N, which is oriented in the SW-NE direction. The major and subsidiary positive anomalies located in the southwestern and southern part of the study area are found at the northward extension of the Corbetti caldera toward the Shala caldera. The cause of these positive anomalies south of Shalla caldera is the Corbetti caldera that forms the southern water divide of the study area. In most part of this area the local negative anomalies are surrounded by the positive anomalies. Most of these anomalies belong to the southern end of Shala-Corbetti segment of the WFB. These positive anomalies may be attributed to the presence of hot ground and fumarolic activity exhibited in the northern part of Corbetti cadera. All geothermal activity south of Shalla caldera may be the result of Corbetti caldera. There is positive anomaly between 450000E and 460000E, which extends up to the Eastern Shalla fault system oriented in the N-S

direction.

Anomaly B

This anomaly includes Shalla caldera, southwestern and southern part of lake Abijata following the orientation of positive anomalies. There is a high residual broader Bouguer anomaly located at the NW part of lake Shala trending SW-NE which are clearly observed in the Bouguer anomaly map. This broad residual Bouguer anomaly is found in the Northwest Shalla Volcanic Boundary, which partly corresponds, to the Southwestrn Danga Volcanic Boundary of lake Abijata Basin. It is formed by rhyolitic-type pumice related to the Tulu Fike cone that result from subaquitic eruptions. This is an indication that the intensive positive anomalies along the rift trend are near surface effects. This may be due to the regional structural feature, such as the WFB and regional rift trending, i.e., NNE-SSW. These enhancing features clearly indicate the continuation of the rift trend NE-SW. The fissural lavas of basic and intermediate composition may be the cause of this observed anomaly.

There is a circular and elongated positive residual gravity anomaly at the southwestern and southern part of lake Abijata oriented in the NW-SE direction and changes its orientation at the southeastern coast of lake Abijata N-S direction. This positive anomaly corresponds to southwestern danga volcanic boundary that forms a large volcanic complex between the Abijata and Shalla lakes. The cause of this positive anomaly may be ascribed to the oldest outcropping volcanics that is the "strongly welded green" and the "weakly welded beige" ignimbrites and thermal feature of surface. This positive anomaly changes its orientation to N-S at the southeastern coast of lake Abijata system and at the eastern Shalla is intersected by a certain geologic structure which pass through the Eastern Shalla fault system and extended to the southern part of study area. The extension this of positive anomaly from the northwestern part of lake Abijata to the southern

margin of study area shows the presence of similar geologic structure and interconnected trending fault system, which play important role for the movement groundwater and geothermal activity in the study area. In general these intensive positive anomalies are found to be associated with the axial zones of recent faulting (WFB), volcanism, and geothermal and seismic activity. There is an E-W trending negative residual anomaly at the northern part of Shalla caldera caused by the recent volcanics of Tulu-Billa basaltic cinder cone and subaqueous volcanics described as "lacustrine guyots" which form the Lencha Gudo and Lencha Tiko cones on the southern shore of lake Abijata.

There is an elongated negative residual gravity anomaly located at the western, southern and eastern part of lake Shalla, which clearly indicates the existence of geologic structure between the wall of the Shalla caldera and its surrounding. At the western part of Shalla caldera this negative residual anomaly that follows the orientation pattern of NE-SW and at the southwestern of lake Shalla change its orientation NW-SE and again at the southeastern of lake Shalla follows an orientation pattern of NE-SW which clearly indicates the continuation of the rift trending NE-SW. This negative anomaly may be caused by the 12Km-wide, submeridian fault system of the Shala-Corbetti segment of the WFB, which includes the Eastern and Southern Shalla fault system (Tiercelin et al, 1997). The negative residual anomaly located at the western part of Lake Shala corresponds to a NNE-trending elongated tectonic depression with a relatively flat and shallow floor belonging to the northern end of the Shala-Corbetti segment of the WFB. In this area the existence of the Southern and Eastern Shalla fault systems play an important role for the flow of groundwater to the lakes and the geothermal activity at the Shalla caldera.

At the eastern coast Shalla caldera after the removal of the regional anomaly, positive local anomalies appeared which are not indicated on the Bouguer anomaly map. The maximum lake

sediments and rift volcanoes in the area may mask this positive anomaly on the Bouguer anomaly map. These positive local anomalies coincide with the hot springs of eastern coast of Shalla caldera. This positive local anomaly indicates the presence of local geothermal field in the area. At the southeastern coast of Shalla caldera similar to the Bouguer gravity anomaly map there is an elongated and broad negative local anomaly following an orientation pattern of NE-SW segment of the WFB. This negative local anomaly coincides with the hot springs found at the southeastern coast of Shalla caldera. Vapour-dominated geothermal field above the convective hydrothermal systems manifested in the area may cause this local negative anomaly.

Anomaly C

This anomaly includes the northern and northeastern part of lake of Abijata; northern, northwestern, western and southern part of lake Langano; eastern and southeastern part of lake Shalla. In the northern and northeastern part of the study area most of the local negative gravity anomalies are similar to the negative Bouguer anomaly map except that the local positive gravity anomaly of the Alutu caldera extended up to the Oitu Bay, most of the northern part of Lake Langano. This positive local anomaly centred at the Aluto-Langano geothermal field is related to the Aluto volcanic centre and underneath the volcano a denser mass seems to be the causative body for the gravity high. This anomaly may be caused by a denser body under the Oitu Bay, where viscous lava is extruded from within at the northern end of lake Langano. This anomaly is pushing into the Aluto volcano. It may be that the two causative bodies have the same root, but the anomaly of the Aluto volcano may have been identified by its low-density volcanics.

There is also another local positive anomaly at the southern part of lake Langano between latitudes of 810000 N and 830000 N that appeared on the residual anomaly map. The gravity data also indicate a small positive gravity anomaly that begins at the southern end of lake Langano and

develops northeastward, culminating in a strong anomaly at the northern end of lake Langano Basin (Searle & Gouin, 1972). The characteristics of this positive anomaly lying below the lake Langano Basin, compared to the other positive and negative anomalies identified in this area, suggest that no thick pile of sediments fills the Langano graben.

Similar to the Bouguer gravity anomaly, the residual Bouguer gravity anomaly shows the same trend and continuity from the northern up to the southeastern part of the study area. The negative anomalies over the rift trough may be a result of the infilling of low density alluvial, lake and volcanic sediments overlying the volcanic sequence of mean density 2.67 gm/cm^3.

Anomaly D

The Bouguer gravity anomaly and the local anomaly are nearly the same.

5.2.4 Bouguer Regional Anomaly Map

The Bouguer regional map (Fig. 10) is obtained with a contour interval of 5 mgal. The same procedure for producing the Bouguer anomaly map is used to obtain the Bouguer regional anomaly map. The separation of the regional Bouguer anomaly, from the residual Bouguer anomaly is based on the wavelength of the anomaly under consideration. The regional Bouguer anomaly is taken above wavelength of 33 Km.

The regional variations that have long wavelength and low amplitude are perceptible over large distances and are thought to be generated by a broad crustal structures at relatively deep-seated density contrasts. Other than the broad (large scale) geologic structures, the regional variations (anomalies) may be caused by intra-basement lithologic changes and isostatic effects associated with deep-seated density anomalies.

It contains circular positive anomaly at the centre of the Shalla caldera geothermal field. This

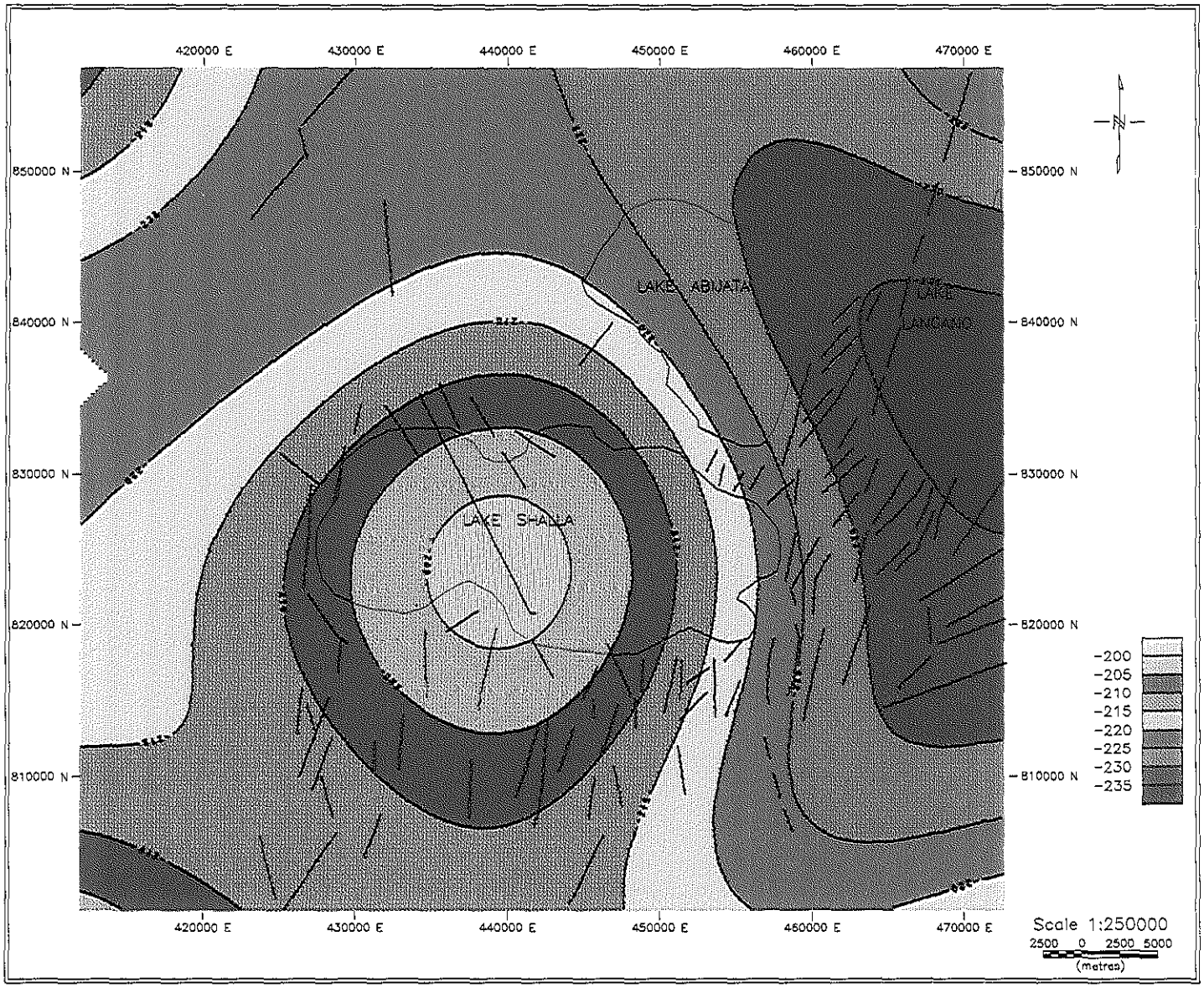

Fig 10. Bouguer regional anomaly map of Shalla caldera and its environs.

regional anomaly may be due to the existence of shallow magma chamber which is responsible for the strong hydrothermal and thermal activities as deduced from surface geologic manifestations of alterations, typical formation of altered rock products exhibited in the area. The regional anomaly increases in a SW direction paralleling the rift axis. This increase can be attributed to the updoming of the asthenospheric high-density material relative to normal mantle in these regions because of more lithospheric attenuation under the rift. There are two other subsidiary positive anomalies located at the NW and SW corner of the study area. The positive anomaly at the SW corner is regional to the Corbetti caldera. The positive anomaly in the NW corner is regional to the Gademotta caldera.

Similar to the continuity of negative Bouguer gravity anomaly in the northern, eastern and southeastern part of the study area is completely covered by the long wavelength negative regional Bouguer anomaly, which indicates the existence of similar structural trend. One can conclude from the orientation of this negative anomaly, this structural trend is an extension and integral structure of the eastern escarpment. The eastern and northeastern part is more negative which could be due to thick low-density asthenospheric material relative the crust emplaced as isostatic compensation under the eastern plateau at the base of the lithosphere, which supports the explanation of a more negative Bouguer anomaly over the eastern plateau. The Bouguer regional anomaly map shows a unification of two separate effects such that across the rift depth to anomalous asthenosphere is significant while along the rift depth to high-density diapers into crust is prominent.

CHAPTER SIX

DISCUSSION, CONCLUSION AND RECOMMENDATION

6.1 DISCUSSION

The end result of a gravity survey is a compilation of gravity anomaly map of the study area considered using the point gravity anomaly values computed at each observation point. Point gravity anomalies are anomaly values computed at each observation point after applying the necessary reductions. Thus, the point gravity anomalies represent the variations of observed gravity at each observation point. Point gravity anomaly of a given survey area are conventionally displayed on gravity profiles or as gravity anomaly map. The gravity profiles represent the variation of the observed gravity field with depth along the selected lines. The gravity anomaly maps represent the variation of the observed gravity field from point to point anywhere within the survey area arising from relatively small density differences between the formations.

The study of gravity anomaly field variations from point to point within the limits of the study area is one of the basic problems of gravimetric survey that is carried out for the purpose of solving problems related to geology. The pattern of variations in the observed gravity field is depicted by the pattern of gravity anomaly maps. These patterns of variations in the observed gravity field are the signatures on the earth's gravity field that are produced by the density contrasts of rock units making up different geologic structures. These signatures reveal the combined gravitational attraction of several structures. Therefore, a gravity anomaly map shows the superposition of relatively sharp anomalies of shallow origin which are caused by near surface noise (effects of shallow masses) or superficial disturbances which is removed by filtering short wavelength anomalies, anomalies with intermediate dimensions caused by small geologic structures that may indicate the most probable geologically interesting sources and very broad anomalies of a regional

nature caused by the effects of deeper masses which may have their origin far below the section within which the geological interest lies. Therefore, gravity interpretation begins with the residual and regional separation.

Groundwater flow and geothermal activity in the rift is controlled by geologic structures, either in a direct way by flow in the tensional faults, fractures and volcanic vents, or through the fluvio-deposits whose occurrence is influenced by tectonism. Three sets of faults which serve as conduits of groundwater flow and geothermal activity were identified in the study area: NE-SW, NW-SE and N-S trending fault systems. The orientation and the relative abundance of these three sets of faults are believed to be the most representative of the fractured part within the study area. The NE-SW and N-S trending faults are sub-parallel, their number of effective intersection is low and they are axial to the rift valley. These two faults serve as the most important source of recharge to the geothermal systems and fracture sets in terms of increasing the permeability and groundwater flow to the rift. However, the overall connectivity of the WFB is increased by the fracture sets NW-SE which intersect the two fault systems. Furthermore, variations in the density and length of NE-SW and N-S trending faults increase their role as conduit for groundwater flow. The groundwater flow through NW-SE is partly tapped by the NE-SW and N-S faults, with the result that groundwater flow southwards through the NE-SW and N-S fault systems from lake Ziway area towards lake Langano and further to the south of lake Shalla. The NW-SE running fractures have limited role as conduits for important groundwater flow. The intersection or cross faulting of NE-SW/N-S with NW-SE trending fault systems may influence or impede the movement of groundwater or facilitate the formation of shallow, young magmatic intrusions where the rhyolites are formed by differentiation. This shallow, young magmatic intrusion, which is manifested as hot springs and fumaroles, is the most important heat source for the geothermal field exhibited at the

Shalla caldera. Therefore, the location of many hot springs and other hydrothermal manifestations is controlled by very young and commonly superficial faults and fault intersections. The most important factor for the formation of geothermal fields is young magmatic heat source at high crustal levels, the hydrothermal circulation of meteoric water in fault/fracture systems, and irregularities in the conductive heat transfer.

According to Craig et al., (1977) the geothermal systems in the Ethiopian rift valley are associated with deep fault-controlled meteoric water. The rift is a region of positive thermal anomalies within which the thermal manifestations are associated with volcanism and seismically active zones. Local geothermal anomalies of direct volcanic association are due to heat flow from shallow magma. These are closely related to the spreading rift zones as evidenced by the alignment of fumaroles and volcanic vents along active fault systems.

The shallow magma chambers which act as source of heat for local geothermal field are either basaltic magma or silicic magma. Basaltic magmas originate from mantle material by partial melting. If basaltic magmas rise directly to the surface forming dykes and thin sheets, they dissipate their heat content rapidly in cooling volcanic products without forming shallow magma chamber. On the other hand, if they solidify near the base of the crust in the extensional regimes by forming shallow magma chambers, they greatly enhance the regional heat flow, which in turn can trigger hydrothermal convection along the steep fault systems created by extensional regimes. In this case, the shallow basaltic magma chambers can have considerable geothermal potential in developing hydrothermal systems.

This case of basaltic magma chamber as source of heat for the geothermal field may be related to the circulation systems with deep fault controlled meteoric water in areas high to normal regional heat flow which is characterized by the springs discharges in fault/fracture zones, especially where

these encounter low topographic. Recharge of such systems occurs preferentially along the fault zones as well. This high regional heat flow often arises from the anomalous thermal processes at the base of the crust. The general crustal setting of such circulation systems is characterized by the number of geological and geophysical features such as low average elevations and consequently high Bouguer gravity anomalies, thin crust and low compressional wave velocity immediately below the crust-mantle boundary, high electrical conductivity and shallow Curie isothermalism. This may be related with the positive Bouguer anomaly located at the southern coast of Shalla caldera and Chitu crater. Furthermore, this area is characterized by the maximum value of regional Bouguer gravity anomaly caused by the homogenous crust of variable density and thickness. The heat source for the geothermal field may be caused by magma chamber of deep origin.

Silicic magmas can be generated by partial melting of mantle material as well as by differentiation of basalts but usually some kind of remelting of crustal material involved. Silicic magma has higher viscosity than basaltic magma and is likely to lodge in the upper crust to form shallow magma chambers and thus act as heat source for substantial duration. Generally long-lived thermal anomalies are supported by silicic magmas than basaltic magmas.

The shallow, young silicic magmatic intrusions related to convective hydrothermal systems may be indicated by the hot springs found at the eastern and southeastern coast of Shalla caldera and hot springs located at the northern coast of lake Langano. The large fault-controlled hot springs located at the eastern coast of Shalla caldera and northern coast of lake Langano is clearly indicated by the positive residual gravity anomaly and the presence of negative gravity anomaly relative to the adjacent terrain is due to the steam fraction in the high-porosity reservoir rocks as well as to the lowered density caused by thermal expansion. The geothermal field exhibited in these area may be caused by a convective hydrothermal systems related to shallow, young silicic

intrusions. The large faulted-controlled hot springs located at the southeastern coast of Shalla caldera coincide with the negative Bouguer and residual gravity anomalies. The geothermal field exhibited in this area may be caused by the vapour-dominated convective hydrothermal systems as clearly indicated by the negative gravity anomaly, several factors like silicification by self-sealing may mask the negative anomalies and can even lead to a positive gravity anomalies above the convective hydrothermal systems.

In general the study area is characterised by short wavelength positive Bouguer gravity anomaly of the Ethiopian rift. The observations define a line of positive residual gravity anomalies due to the mass excesses below the rift floor associated with strong hydrothermal activities in the rift. There is strong correlation between the positive residual gravity anomalies in the rift following the strike of the WFB, the geothermal activity and the location of Quaternary siliceous domes and recent fissural basalt flows. The root of the denser fissural basalts may still be hot and the siliceous domes of the Shalla caldera geothermal field with strong hydrothermal manifestations more likely have hot basaltic dikes underneath associated with their magma chambers that feed their thermal features. In general, all the geothermal activity north of the Shalla caldera may be related to the Aluto-Langano geothermal field through the recent complex volcanic structures and the active trending fault system. Similarly, the geothermal activity south of Shalla caldera may be ascribed to the Corbetti caldera through the Shalla-Corbetti segment of the Wonji Fault Belt.

The present study shows that local geothermal manifestations are aligned along the recent active Wonji Fault Belt and central volcanic complexes. The most important geothermal fields are localised around Aluto close to lake Langano and the Shalla caldera that are associated with strong positive gravity anomalies. This may show the relation of heat source to denser intrusive mantle derived sources at a relatively shallow depth.

6.2 Conclusions

The main conclusions are:

The Buoguer gravity anomaly map shows a series of linear maxima and minima superimposed on the broad regional negative anomaly. Each linear feature is indicated by steep and horizontal gravity gradients. The steep gravity gradient is an indicative of faulting while the high horizontal gradient is an indicative of contact between rock units having different density contrast.

Bouguer gravity anomaly suggests that the basement topography comprises of a series of alternating fault-bounded horst and graben structures, which define a rift system in the study area striking NE-SW, NW-SE and N-S.

The negative and positive gravity anomalies are attributed to sediment/basement interface density contrasts. The negative anomalies are interpreted as low-density sediments overlying denser basement rocks or as small extent sedimentary basins or due to relatively light acidic intrusions. The positive gravity anomalies are caused by high density intrusions (heavy basic intrusions) and intrusions associated with the WFB. The crust is thinner beneath these positive anomalies due to the presence of high-density intrusive at Shala caldera.

The most prominent feature observable from the residual Bouguer anomaly map is the strong correlation of the positive gravity anomalies in the rift, strike of the Wonji Fault Belt, the geothermal activity, and Quaternary siliceous domes and recent fissural basalts.

The circular positive regional Bouguer anomaly at the centre of the Shalla caldera geothermal field may be due to the high-density magma chamber of shallow origin, which causes thin and shallow maximum heating of the crust responsible for the hydrothermal activity of Shalla caldera.

The WFB is a linear zone along which recent lavas and ignimbrites have erupted and the whole volcano-tectonic association is suggestive of crustal tension acting across the rift. The displacement

lines of Wonji fault belt are sites of shallow crustal heating, thin crust and consequently high Bouguer gravity anomalies which is attributed to the geothermal activity at each silicic volcanic centres in general and Shalla caldera in particular.

The heat source responsible for the formation of the geothermal field at Shalla caldera may be caused by either shallow, young magmatic intrusions that are probably facilitated by cross faulting where the rhyolites are produced by differentiation or high regional heat flow in deep fault-controlled meteoric water which arise from the anomalous thermal processes at the base of the crust.

5.3 Recommendation

Based upon investigations made under this study the following recommendations are forwarded:

1) Although the gravity data interpretation has revealed plenty of new information, the data was previously processed by other workers. Since the data was collected on randomly distributed transverse patterns some of the data might be highly scattered while at other places there could be sufficient data density. Consequently when the data is processed the gap between the highly scattered data points and the densely distributed data points will be filled up by interpolation, hence, new data was created. During previous data processing phase it is believed that some of the original data quality could have been affected due to the process of interpolation. It is better to work on the original data.

2) Integrated geophysical work such as reflection and refraction seismic, electrical resistivity method and reprocessing and interpretation of previous data collected in the regions adjacent to the present study area is essential since these areas are a potential source for the economic development of the country.

REFERENCES

Abera Alemu, 1983. Crustal Modeling from Gravity Data in the Ethiopian Rift. M.Sc. Thesis, Addis Ababa University, Addis Ababa, Ethiopia.

Baker, B.H, Mohr, P.A. and Williams, L.A.J., 1972. Geology of the eastern rift system of Africa. Geol. Soc. Am. Spec. Pap., 136:67pp.

Baumann, A., Forstner, U., & Rhode, R., 1975. Lake Shala: Water Chemistry , mineralogy and geochemistry of sediments in an Ethiopian rift lake. Geol. Rundsch., 64, 593-609.

Di Paola, G.M. 1972. The Ethiopian Rift Valley (between 7° and 8° lat. North. Bull.Vulcan.,36. 517-560.

Dobrin, M.B.,and Savit, C.H., 1988. Introduction to Geophysical prospecting. McGraw-Hill Inc. Singapore.

Ebinger, C.J., Yemane. T., WoldeGabriel, G., Aronson, J.L., & Walter, R.C 1993. Late Eocene-Recent Volcanism and faulting in the southern main Ethiopian rift. J. Geol. Soc., London, 150, 99-108.

Gianelli, G., & Teklemariam, M. 1993. Wate-rock interaction processes in the Altu-Langano geothermal field (Ethiopia). Journal of Volcanology and Geothermal Research, 56, 429-445.

Gibson, I., L., 1969. Structural and geology of an axial portion of the Main Ethiopian Rift. Tectonophysics 8: 561-568.

Kazmin, V., Berhe, S.M., 1978. Geolgy and development of Nazerath area, Northern Ethiopian Rift. EIGS, Note number 11, Addis Ababa, Ethiopia.

Kazmin, V., 1979. Stratigraphy and correlation of volcanic rocks in Ethiopia. EGIS, Note number 106: 1-26.

Kazmin, V., Berhe, S.M., Nicoletti, M., & Petrucciani, C., 1980. Evolution of the northern part of the Ethiopian rift: Sheet NC 37-15, Momoir number 3, 26 pp.

L. Rybach and L.J.P. Muffler , 1981. Geothermal Systems: Principle and Case Histories.

Lloyd, E.F. 1977. Geologiucal factors influencing geothermal exploration in the Langano Region, Ethiopia ,Unpubl. MS., 73 pp.

Meyer, W., Pilger, A., Rosler, A., & Stets, J. 1975. Tectonic evolution of the northern part of the main Ethiopiain rift in Southern Ethiopia. In: Afar Depression of Ethiopia (Ed. by

A.Pilger& A. Rosler), pp. 352-362. Stuttgart: Inter-Union commission on Geodynamics, Sci. Rpt. 14.

Mohr, P., Mitchell. J.G., & Raynolds, R.G.H. 1980. Quaternary Volcanism and Faulting at O'a Caldera, Central Ethiopian Rift. Bull. Volcanol. , 43-1, 173-189.

Mohr, P.A., 1960. Report on a geological excursion through southern Ethiopia: Bull. Geophys. obs. Addis Ababa, no. 3, p. 9-20.

Mohr, P.A., 1967a. The Ethiopian rift system: Bull. Geophys. Obs. Addis Ababa, no. 11, p. 1-65.

Mohr, P.A., 1967c. Major volcano-Tectonic lineament in the Ethiopian rift system: Nature, V. 213, p. 664-665.

Morelli,C., Ganta, C., Honkasalo, J., McConnell, R.H., Tanney, I.G.,Sgabo,B., Uotila, U. and Whalen C.T., 1971. The International Standardization Gravity Net 1972, IAG, 39 terrue Gray Lussac, 75005, Paris.

Mortiz, H., 1971. Geodetic References System 1967. Pub. No.3, Bulletin Geodesique, Paris.

Searle, R.C and Gouin, P., 1972. A Gravity Survey of the Central Part of the Ethiopian Rift Valley. Tectonophysics. 15:41-52.

Street, F.A. 1979. Late Quaternary lakes in the Ziway -Shala Basin , Southern Ethiopia . Ph. D, Cambridge.

Tenalem Ayenew, 1998. The hydrological system of the Lake District Basin, Centrral Main Ethiopian Rift. PhD. thesis. ICT Publication, Number 64.

Torge, W., 1989. Gravimetry, Walter de Gruyter & Co., Berlin, Germany.

Tiercelin, J.-J., Caroline Le Turdu & Francoise Gasse 1997. International Symposium "Flood Basalts, Rifting and Paleoclimates in the Ethiopian Rift and Afar Depression" Addis Ababa, Ethiopia February 3 to 14,1997 (unpublished).

UNDP 1973. Investigation of Geothermal Resources for Power Development: Geology, Geochemistry and Hydrology of the Hot Springs of the East African Rift System Within Ethiopia .(Tech. Rpt. DP/SF/UN/116 No. 275 pp.) UNDP, New York.

WoldeGabriel, G., Aronson, J.L. & Walter, R.C 1990. Geology ,Geochronology, and rift basin development in the central sector of the Main Etiopian Rift. Geological Society of American Bulletin , 102, 439- 458.

WoldeGabriel, G., Walter, R.C., Aronson, J. L., Hart, W. K. 1992. Geochronology and distribution of silicic volcanic rocks of Plio-Pleistocene age from the central sector of the Main Ethiopian Rift. Quaternary International , 13/14, 69-76.

WoldeGabriel, G. 1987. Volcanotectonic history of the central sector of the Main Ethiopian Rift . Ph. D. thesis, Case Western Reserve Univ. , Cleveland, Ohio, 410 pp.

WoldeGabriel, G., Yemane, T., Suwa , G., White, T. & Asfaw, B. 1991. Age of volcanism and rifting in the Burji-Soyoma area, Southern Main Ethiopian Rift : Geo- and biochronological data. Journal of African Earth Sciences, 13, 437-447